ARTICLE

The STX17-SNAP47-VAMP7/VAMP8 complex is the default SNARE complex mediating autophagosome–lysosome fusion

Fenglei Jian[1,5], Shen Wang[2,5], Rui Tian[1], Yufen Wang[1], Chuangpeng Li[1], Yan Li[3], Shixuan Wang[3], Chao Fang[1], Cong Ma[2]✉ and Yueguang Rong[1,4]✉

© The Author(s) under exclusive licence to Center for Excellence in Molecular Cell Science, Chinese Academy of Sciences 2024

Autophagosome–lysosome fusion mediated by SNARE complexes is an essential step in autophagy. Two SNAP29-containing SNARE complexes have been extensively studied in starvation-induced bulk autophagy, while the relevant SNARE complexes in other types of autophagy occurring under non-starvation conditions have been overlooked. Here, we found that autophagosome–lysosome fusion in selective autophagy under non-starvation conditions does not require SNAP29-containing SNARE complexes, but requires the STX17-SNAP47-VAMP7/VAMP8 SNARE complex. Further, the STX17-SNAP47-VAMP7/VAMP8 SNARE complex also functions in starvation-induced autophagy. SNAP47 is recruited to autophagosomes following concurrent detection of ATG8s and PI(4,5)P_2 via its Pleckstrin homology domain. By contrast, SNAP29-containing SNAREs are excluded from selective autophagy due to inactivation by O-GlcNAcylation under non-starvation conditions. These findings depict a previously unknown, default SNARE complex responsible for autophagosome–lysosome fusion in both selective and bulk autophagy, which could guide research and therapeutic development in autophagy-related diseases.

Cell Research (2024) 34:151–168; https://doi.org/10.1038/s41422-023-00916-x

INTRODUCTION

Autophagy is responsible for nutrient recycling and clearing damaged or excess organelles and protein aggregates from cells, thus functioning as a fundamental process in quality control and cellular homeostasis.[1–4] Deficiencies or defects in autophagy are associated with many human disorders, particularly those related to neuron degeneration or metabolic diseases.[3,4] Accumulating studies have demonstrated that autophagosomes selectively recognize substrates for degradation via specific receptor proteins located on the membrane of organelles in selective autophagy.[1,5] These receptor proteins link substrates to autophagosomes to ensure the specificity of autophagic degradation.[1,5] However, the mechanism underlying autophagosome–lysosome fusion in selective autophagy under non-starvation conditions remains unknown.

The SNARE complex (composed of Qa, Qb, Qc, and R-SNAREs) localizes to the outer membrane of vesicles and is responsible for membrane fusion.[6] To date, two SNARE complexes have been identified in autophagosome–lysosome fusion in the context of starvation-induced bulk autophagy. The first is composed of STX17, SNAP29, and VAMP7/VAMP8[7,8] where the Qa-SNARE STX17 translocates to sealed autophagosomes during autophagy and interacts with the cytosolic Qbc-SNARE SNAP29 and lysosomal R-SNARE VAMP7/VAMP8 to form a ternary SNARE complex that mediates autophagosome–lysosome fusion.[7–9] Incomplete blocking of autophagosome–lysosome fusion in STX17 knock-out (KO) mammalian cells led to the discovery of a second SNARE complex (YKT6-SNAP29-STX7) for autophagosome–lysosome fusion.[10] In this case, YKT6, the R-SNARE in this complex, is recruited to autophagosomes via the N-terminal longin domain and the Qa-SNARE STX7 localizes to lysosomes. Depletion of any single component of these two SNARE complexes will partially inhibit autophagosome–lysosome fusion. Lack of both STX17 and YKT6 almost completely blocks autophagosome–lysosome fusion in starvation-induced autophagy.[10] Notably, YKT6 is also involved in autophagosome–lysosome fusion in *Drosophila* and *Saccharomyces cerevisiae*, but functions through different mechanisms.[11–13] However, it has thus far remained completely unknown whether the SNAP29-containing SNARE complexes that mediate autophagosome–lysosome fusion are also involved in selective autophagy under non-starvation conditions.

Here, we found that an unidentified default SNARE complex, STX17-SNAP47-VAMP7/VAMP8, mediates autophagosome–lysosome fusion in selective autophagy under non-starvation conditions, rather than the SNAP29-containing SNARE complexes (STX17-SNAP29-VAMP7/VAMP8 and YKT6-SNAP29-STX7) that are active in starvation-induced bulk autophagy. In this fusion process, SNAP47, rather than SNAP29, is recruited to phagophores (where it remains throughout the autophagosome stage) via concurrent binding of PI(4,5)P2 and ATG8s with its PH domain. SNAP29 O-GlcNAcylation blocks SNAP29 recruitment to autophagosomes, subsequently allowing SNAP47 to occupy autophagosomal STX17 in selective autophagy under non-

[1]School of Basic Medicine, Tongji Medical College and State Key Laboratory for Diagnosis and Treatment of Severe Zoonostic Infectious Disease, Huazhong University of Science and Technology, Wuhan, Hubei, China. [2]Key Laboratory of Molecular Biophysics of the Ministry of Education, College of Life Science and Technology, Huazhong University of Science and Technology, Wuhan, Hubei, China. [3]Department of Obstetrics and Gynecology, Tongji Hospital, Tongji Medical College, Huazhong University of Science and Technology, Wuhan, Hubei, China. [4]Cell Architecture Research Center, Huazhong University of Science and Technology, Wuhan, Hubei, China. [5]These authors contributed equally: Fenglei Jian, Shen Wang. ✉email: cong.ma@hust.edu.cn; rongyueguang@hust.edu.cn

Received: 3 August 2023 Accepted: 11 December 2023
Published online: 5 January 2024

starvation conditions. Ultimately, SNAP47 forms a ternary SNARE complex with STX17 and VAMP7/VAMP8 to mediate autophagosome–lysosome fusion. Further, STX17-SNAP47-VAMP7/VAMP8 SNARE complex also functions in starvation-induced autophagy. Therefore, our study shows that SNAP29-containing SNARE complexes necessary for starvation-induced bulk autophagy are not required for selective autophagy under non-starvation conditions, and identifies a previously unknown default STX17-SNAP47-VAMP7/VAMP8 SNARE complex that instead mediates autophagosome–lysosome fusion in both selective autophagy under non-starvation conditions and starvation-induced autophagy.

RESULTS

SNAP47 primarily localizes to mitophagosomes

In mammals, two SNARE complexes, STX17-SNAP29-VAMP8 and YKT6-SNAP29-STX7, have been shown to be responsible for autophagosome–lysosome fusion during starvation-induced bulk autophagy.[7,8] However, it remains unknown whether these two SNARE complexes are also responsible for autophagosome–lysosome fusion in selective autophagy under non-starvation conditions. Pursuing this question, we individually knocked down SNAP29 (a Qbc-SNARE protein shared in both SNAP29-containing complexes), STX7, or YKT6 in HeLa cells stably expressing Parkin to prevent the formation of these two complexes, and then examined oligomycin and antimycin (OA)-induced mitophagy, the most well-studied form of selective autophagy. Interestingly, neither SNAP29, STX7, nor YKT6 knockdown (KD) was able to prevent degradation of mitochondrial proteins (i.e., PHB2, COX2, TOM20) upon mitophagy induction by OA (Supplementary information, Fig. S1a–d). These results suggest that both STX17-SNAP29-VAMP7/VAMP8 and YKT6-SNAP29-STX7 SNARE complexes are unlikely to participate in mitophagosome–lysosomesome fusion.

To screen for the SNARE complex that mediates mitophagosome–lysosomesome fusion, we first examined the localization of all 39 known SNARE proteins during mitophagy (Fig. 1a). Interestingly, a strong signal of a vertebrate-specific SNARE SNAP47 appeared to envelope mitochondrial matrix protein HSP60, while STX17, VAMP7, and VAMP8 showed lower but obvious envelopment (Supplementary information, Fig. S1e, f). To further confirm the localization of SNAP47 to mitophagosomes, we co-stained SNAP47 and HSP60 with the autophagosomal proteins LC3B or p62 and found that SNAP47 enveloped both HSP60 and LC3B or p62 upon mitophagy induction (Fig. 1b, c). The colocalization of SNAP47 with LC3B and HSP60 could be observed in other cell lines (Supplementary information, Fig. S2a–d). However, SNAP47 did not show obvious colocalization with the lysosome marker LAMP2 upon early mitophagy induction (Fig. 1d). In addition, SNAP47-wrapped HSP60 showed limited colocalization with phagophore markers (WIPI2 and ATG16L1) (Fig. 1e, f). Collectively, these results suggest that SNAP47 primarily localizes to mitophagosomes.

In order to determine whether HSP60 envelopment by SNAP47 could be attributed to SNAP47 localization to the mitochondria surface, we co-stained SNAP47 and HSP60 with the mitochondrial outer membrane protein TOM20. Line profile analysis showed that the SNAP47 signal was detectable outside the TOM20 signal (Fig. 1g, h), thus ruling out SNAP47 localization to the mitochondrial outer membrane. To further confirm this observation, we also examined SNAP47 and TOM20 localization by super-resolution structured illumination microscopy (SIM). The imaging data confirmed that SNAP47 was surrounding but external to TOM20 and LC3 locations (Fig. 1i, j). Correlative light and electron microscopy (CLEM) also indicated a GFP-SNAP47-labeled double membrane structure engulfing the damaged mitochondria (Fig. 1k, l). Together, these results suggest that SNAP47 mainly localizes to mitophagosomes, but not the mitochondrial outer membrane, during mitophagy.

Given that both SNAP47 and SNAP29 belong to the Qbc-SNARE subfamily, and considering that SNAP29 localizes to autophagosomes during starvation-induced bulk autophagy,[7] we next examined whether SNAP29 also localizes to mitophagosomes. In line with our observation that mitochondrial protein degradation was not affected in SNAP29 KD cells (Supplementary information, Fig. S1a), SNAP29 showed no colocalization with LC3/HSP60-double positive puncta in all cell lines we tested (Fig. 1m; Supplementary information, Fig. S2e–h**).**

SNAP47 is required for autophagosome–lysosome fusion in mitophagy

Given the non-trivial localization of SNAP47 on mitophagosomes, we next sought to investigate the potential functions of SNAP47 in mitophagy. Western blotting analysis showed obvious inhibition of mitochondrial protein degradation (TOM20, PHB2, COX2) in SNAP47 KD cells (Fig. 2a; Supplementary information, Fig. S3a–d), while their mRNA levels were not impacted (Supplementary information, Fig. S4a, b). Previous studies have shown that mito-Keima, a pH sensitive mitochondria-targeting chimera protein, has dual excitation peaks in its protonated and deprotonated states, providing a ratiometric and reversible measure of pH when mitochondria engulfed by autophagosomes are delivered to acidic lysosomes.[14] Here, the mito-Keima fluorescence conversion was also inhibited in SNAP47 KD cells upon mitophagy induction by OA (Fig. 2b, c, g, h; Supplementary information, Fig. S4c, e). In contrast, mitochondrial protein degradation and mito-Keima fluorescence conversion under SNAP29 KD were indiscernible from those in wild-type (WT) cells (Fig. 2d–h; Supplementary information, Figs. S3e–h and S4d, e). SNAP29/SNAP47 double knock-out (DKO) did not further inhibit mitochondria proteins degradation compared to that in SNAP47 KO cells (Fig. 2i). In addition, SNAP47 depletion also led to decreased colocalization between LAMP2 and HSP60 in mitophagy and increased LC3 puncta accumulation, compared to those in control cells (Supplementary information, Fig. S4f–i), while the colocalization of WIPI2 with HSP60 in SNAP47 KO cells is similar to that in WT cells, suggesting that SNAP47 KO has no effect on mitophagosome formation (Supplementary information, Fig. S4j, k). Together, these results suggest that SNAP47 is required for autophagosome–lysosome fusion in mitophagy.

To further confirm the role of SNAP47 in mitophagy, we generated five independent SNAP47 KO clones in HeLa cells. Consistent with the findings above, the degradation of mitochondrial proteins was inhibited under SNAP47 KO (Fig. 2j), while the inhibition of mitochondrial protein degradation was abolished in WT SNAP47-complemented cells (Fig. 2k). We found that SNAP47 KO did not affect lysosomal cathepsin D processing and lysosomal acidity (Supplementary information, Fig. S4l, m), suggesting that SNAP47 depletion does not lead to lysosomal dysfunction. Cumulatively, these results strongly suggest that SNAP47, but not SNAP29, is required for mitophagosome–lysosomesome fusion in OA-induced mitophagy.

Akin to OA-induced mitophagy, SNAP47 colocalization with LC3 and HSP60 was observed in hypoxia-induced mitophagy (Fig. 2l) and mitochondrial protein degradation was inhibited in SNAP47 KO cells, which could be reversed by re-expression of WT SNAP47 (Fig. 2m). These results suggest that SNAP47 also participates in hypoxia-induced mitophagy.

SNAP47 also functions in other types of selective autophagy

We also tested the role(s) of SNAP47 in other types of selective autophagy. First, we examined two models of aggrephagy in Hela cells, including puromycin-induced protein aggregation[15–17] and HTT-Q103 mutant protein aggregation.[18] In both models, SNAP47, rather than SNAP29, clearly co-localized with ubiquitin-labeled aggregates or HTT-Q103 aggregates (Supplementary information, Figs. S5a–c, S5g–i, S6a–c, S6f–h and S7a–c). Furthermore, SNAP47

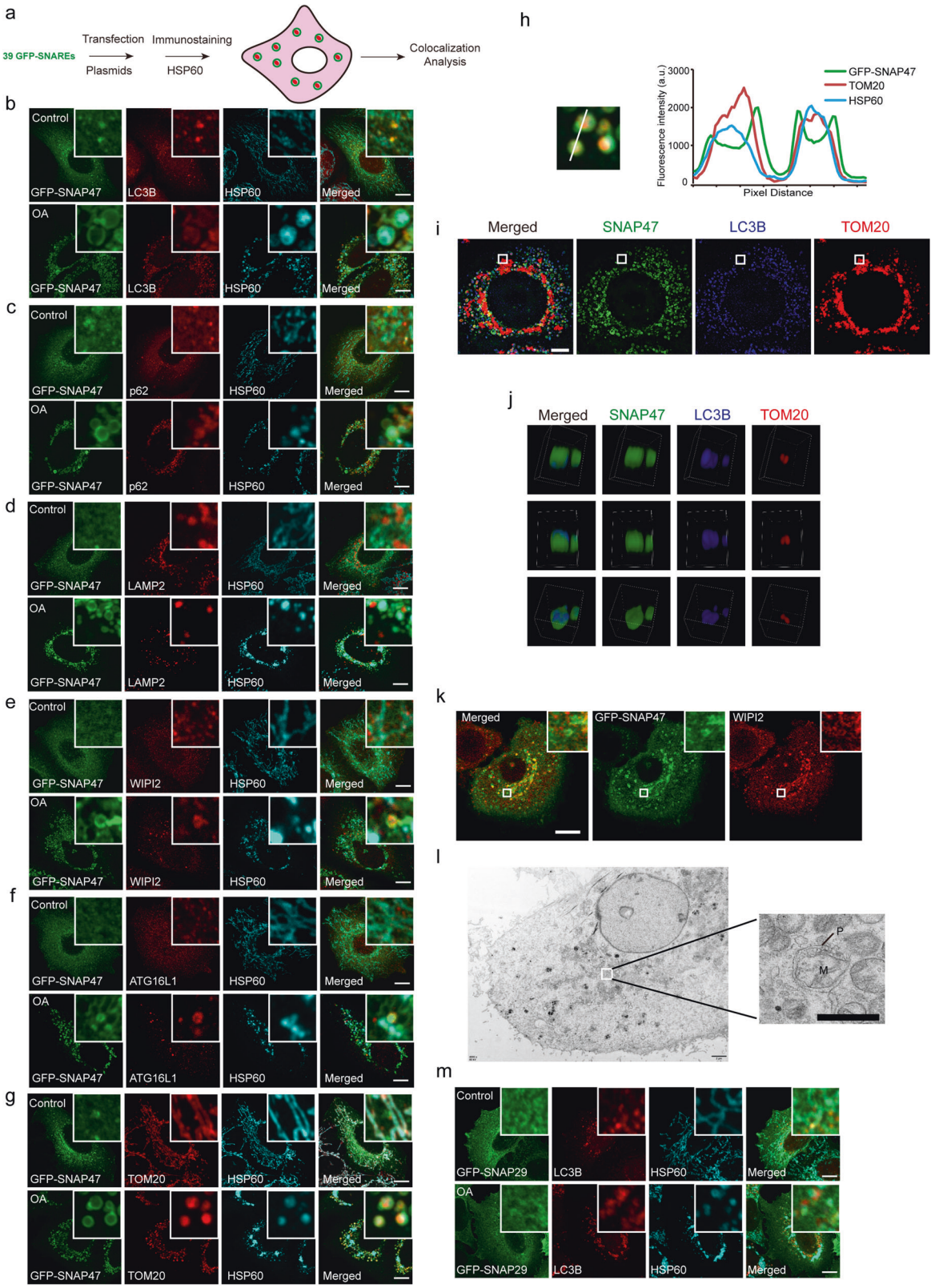

depletion, but not SNAP29 depletion, resulted in markedly inhibited degradation of protein aggregates in response to puromycin treatment or HTT-Q103 mutation (Supplementary information, Figs. S5d–f, j, k, S6d, e, i, j and S7d, e).

Similarly, in thapsigargin-induced ER-phagy, SNAP47 co-localized with the ER-phagy receptors, FAM134B and LC3, while SNAP29 did not (Supplementary information, Fig. S8a–d). Moreover, the degradation of the ER-phagy substrates, FAM134B and

Fig. 1 SNAP47 primarily localizes to mitophagosomes. a The schematic diagram for SNARE screen. **b**–**f** HeLa cells stably expressing Parkin (HeLa/Parkin cells) were transfected with GFP-SNAP47. Twenty-four hours after transfection, cells were treated with DMSO or OA (oligomycin 2.5 μM and antimycin-A 250 nM) for 4 h, and then were stained with indicated antibodies. Scale bars, 5 μm. **g**, **h** HeLa cells stably expressing Parkin and GFP-SNAP47 were treated with DMSO or OA for 4 h and then stained with anti-TOM20 and anti-HSP60 antibodies (**g**). Scale bars, 5 μm. Line profile analysis of the signal intensity of GFP-SNAP47, TOM20 and HSP60 along the line (**h**). **i**, **j** HeLa cells stably expressing Parkin and GFP-SNAP47 treated with OA were stained with anti-TOM20 and anti-LC3B antibodies. Images were acquired using a super-resolution structured illumination microscope. Scale bars, 5 μm. 3D reconstruction images showed GFP-SNAP47 surrounding outside TOM20. **k**, **l** Correlative confocal and TEM images of the same HeLa/Parkin expressing GFP-SNAP47 and mKATE2-WIPI2. Scale bars, 10 μm in the confocal image (**k**). Scale bars, 2 μm in the EM image. An enlarged inset is shown on the right of the EM image. Scale bars, 1 μm (**l**). **m** HeLa/Parkin cells were transfected with GFP-SNAP29. Twenty-four hours after transfection, cells were treated with DMSO or OA for 4 h, and then were stained with anti-LC3B and anti-HSP60 antibodies. Scale bars, 5 μm.

SEC61β, was dramatically reduced in SNAP47-depleted cells, but not in cells with SNAP29 depletion (Supplementary information, Fig. S8e–h). These collective results thus support the role of SNAP47, but not SNAP29, in certain types of selective autophagy under non-starvation conditions.

SNAP47 functions in starvation-induced bulk autophagy

Interestingly, immunostaining revealed that SNAP47 also co-localized with LC3 and p62, but it showed limited colocalization with phagophore markers (WIPI2 and ATG16L1) and the lysosomal protein, LAMP2, in starvation-induced autophagy (Fig. 3a–d). Density gradient fractionation assays showed that SNAP47 co-fractionated with autophagosomal proteins STX17, LC3 and p62 (Fig. 3e). These results suggest that SNAP47 presents on autophagosomes in starvation-induced bulk autophagy. The acidification of RFP-GFP-LC3, indicated by quenching of GFP due to low lysosomal pH, along with the stable RFP and co-localization of LC3 with LAMP2 were significantly inhibited in SNAP47 KD cells upon EBSS starvation (Fig. 3f–j). Consistent with this finding, the degradation of LC3-II and p62 was inhibited in SNAP47 KD or SNAP47 KO cells (Fig. 3k, l), and this inhibition was reversed in SNAP47 KO cells complemented with WT SNAP47 (Fig. 3m). These results together suggest that SNAP47 also participates in autophagosome–lysosome fusion in starvation-induced bulk autophagy.

Given previous reports that SNAP29-containing SNARE complexes are required for autophagosome–lysosome fusion in starvation-induced autophagy,[7,8,10] we speculated that SNAP29 and SNAP47 are redundant in starvation-induced autophagy in mammalian cells. Supporting our hypothesis, we found that the recruitment of SNAP29 and SNAP47 was inter-independent, since the colocalization of LC3 with SNAP29 or SNAP47 was unaffected in SNAP47 KO cells and SNAP29 KD cells, respectively (Supplementary information, Fig. S9a–d). And depletion of either SNAP29 or SNAP47 inhibited the degradation of LC3 and p62 and GFP acidification of RFP-GFP-LC3, but depletion of SNAP29 in SNAP47 KO cells further inhibited the degradation of LC3 and p62 and GFP acidification of RFP-GFP-LC3 compared to those in SNAP29 or SNAP47 single depletion cells (Supplementary information, Fig. S9e–g). These data suggest that SNAP47 plays a redundant role with SNAP29 in autophagosome–lysosome fusion in starvation-induced bulk autophagy. Therefore, SNAP47-containing SNARE complex plays a multi-functional role in both starvation-induced autophagy and selective autophagy under non-starvation conditions, while SNAP29-containing SNARE complexes function only in starvation-induced bulk autophagy. In essence, these findings suggest that SNAP47-containing SNARE complex is the default SNARE complex, generally responsible for autophagy induced by a variety of stress stimuli.

The STX17-SNAP47-VAMP7/VAMP8 ternary SNARE complex mediates autophagosome–lysosome fusion

The SNARE complex is composed of Qa-, Qb-, Qc- or Qbc-, and R-SNAREs.[6] SNAP47 belongs to Qbc-SNARE family. In order to identify possible Qa- and R-SNARE interaction partners of SNAP47, we used co-immunoprecipitation assays to screen for interactions between SNAP47 and Qa- or R-SNAREs. Unexpectedly, we found that SNAP47 interacted with all Qa-SNAREs except for STX1A (Supplementary information, Fig. S10a). Immunofluorescence staining of these 13 SNAREs revealed that signals for STX4, STX5, STX7, STX17, STX18 and STX19 partially colocalized with HSP60 in mitophagy (Supplementary information, Fig. S1e, f). Hence, we knocked down each of the 6 Qa-SNAREs individually and found that only STX17 KD resulted in remarkable inhibition of mitochondrial protein degradation upon mitophagy induction (Supplementary information, Fig. S10b), indicating that STX17 is a likely Qa-SNARE partner of SNAP47. Among the R-SNARE proteins we screened, VAMP4, VAMP5, VAMP7 and VAMP8, but not YKT6, showed obvious interactions with SNAP47 in co-immunoprecipitation assays (Supplementary information, Fig. S10c). However, only VAMP4, VAMP7, and VAMP8 colocalized to HSP60-positive puncta in mitophagy (Supplementary information, Fig. S1e, f), and mitochondrial protein degradation was inhibited upon KD of VAMP7 or VAMP8, but not VAMP4 in HeLa cells (Supplementary information, Fig. S10d, e). These results suggest that VAMP7 and VAMP8 might function together with SNAP47 as R-SNAREs.

We then conducted a series of immunoprecipitation assays to further confirm that SNAP47 can interact with STX17 and VAMP7/VAMP8 (Supplementary information, Fig. S10g–i). The results showed that Flag-SNAP47 also interacted with endogenous STX17 and VAMP7/VAMP8 and vice versa (Fig. 4a; Supplementary information, Fig. S10j–l). Interactions among endogenous STX17, SNAP47 and VAMP7/VAMP8 proteins were also detected (Fig. 4b). In addition, SNAP47 KD decreased interactions between STX17 and VAMP7/VAMP8 (Fig. 4c, d), whereas their interactions were enhanced upon SNAP47 overexpression (Fig. 4e, f). SNAP47 also colocalized with STX17 and LC3 or HSP60 in mitophagy (Fig. 4g, h). Taken together, these results suggest that SNAP47, STX17, and VAMP7/VAMP8 form a ternary SNARE complex following induction of mitophagy.

To verify the function of this SNAP47-STX17-VAMP7/VAMP8 ternary SNARE complex, the in vitro liposome fusion between proteoliposomes reconstituted with STX17 and VAMP7/VAMP8 in the presence of SNAP29 or SNAP47 was examined (Fig. 4i). Similar to the in vitro liposome fusion activity of STX17-SNAP29-VAMP8 observed in previous studies,[9] we found that STX17-SNAP47-VAMP8 and STX17-SNAP47-VAMP7 SNARE complexes also mediate liposome fusion in vitro (Fig. 4j, k). Together, these results strongly suggest that STX17-SNAP47-VAMP7/VAMP8 forms a functional ternary SNARE complex to mediate mitophagosome–lysosomesome fusion.

SNAP47 is recruited to autophagic vacuoles via concurrent binding to PI(4, 5)P_2 and ATG8s

We next used time lapse imaging to determine when SNAP47 is recruited to autophagic vacuoles during the induction of mitophagy. Using HeLa cells, we observed a BFP2-LC3$^+$/mKATE2-WIPI2$^+$/GFP-SNAP47$^-$ vesicle at the initiation of mitophagy induction, and GFP-SNAP47 signal gradually emerged on this vesicle (Fig. 5a) and no dramatic changes on the oblateness of

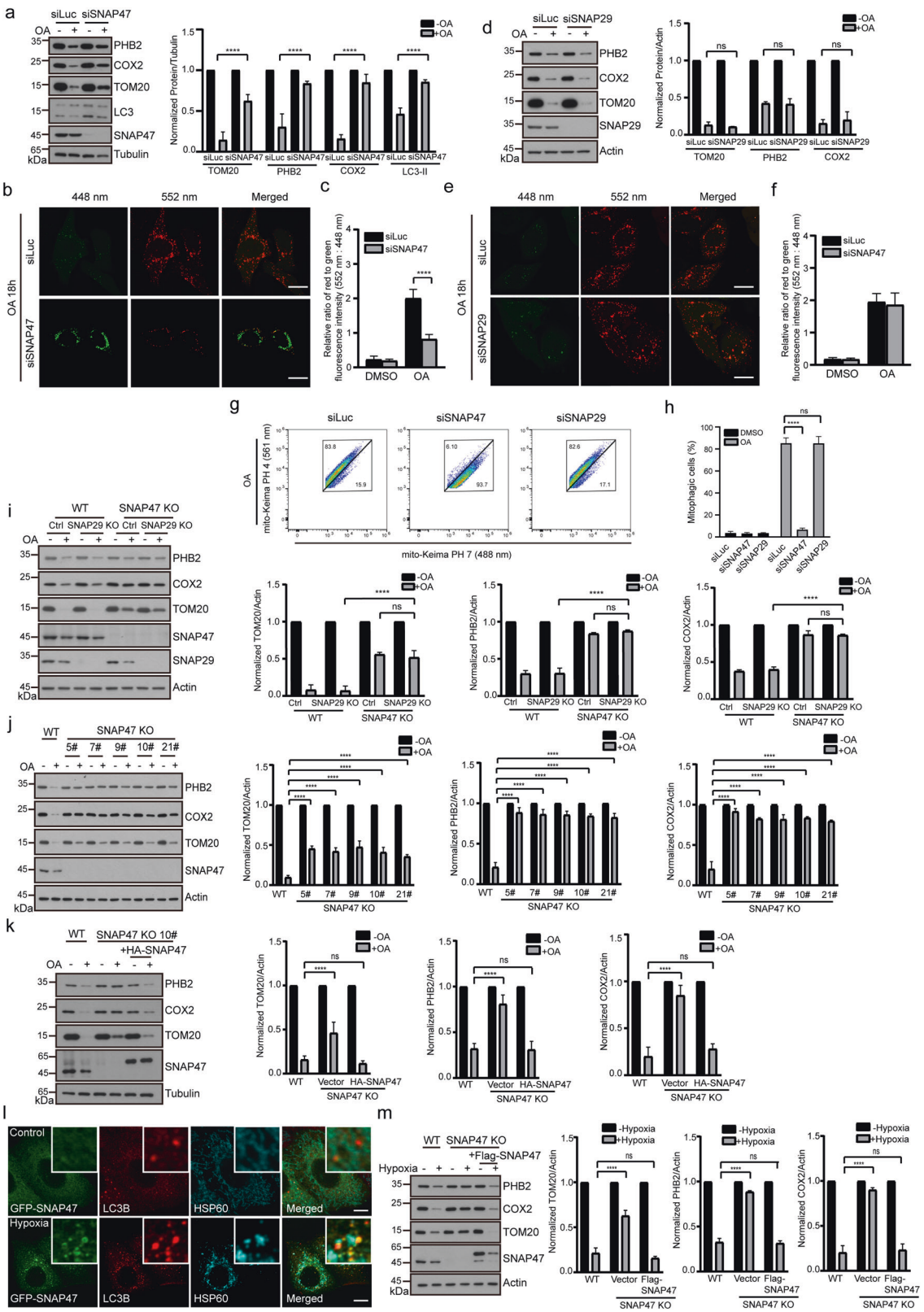

autophagic vacuoles were observed before and after SNAP47 recruitment (Fig. 5b). This result suggests that SNAP47 is first recruited to phagophores, which is consistent with our observations that SNAP47 shows limited colocalization with the isolation membrane markers, WIPI2 and ATG16L1 (Fig. 1e, f).

Since a PH domain was identified on the N-terminal of SNAP47 at the National Center for Biotechnology Information (NCBI) conserved domain prediction (Fig. 5c) and PH domains are reportedly involved in protein targeting to specific organelle membranes via binding different phosphoinositols,[19] we next

Fig. 2 SNAP47 is required for mitophagosome–lysosomesome fusion. a HeLa/Parkin cells were transfected with siLuc (siLuciferase) or siSNAP47. Forty-eight hours after transfection, cells were treated with DMSO or OA for 18 h. Cells were lysed and immunoblotted with indicated antibodies. Quantification of normalized TOM20, PHB2, COX2 and LC3-II in **a**. Data are represented as mean ± SD ($n = 3$, three independent experiments). ****$P < 0.0001$, two-way ANOVA. **b**, **c** HeLa cells stably expressing Parkin and mito-Keima were transfected with siLuc or siSNAP47. Forty-eight hours after transfection, cells were treated with OA for 18 h. Live cells were analyzed by confocal microscopy. Scale bars, 10 μm. The relative ratio of fluorescence intensity (552 nm:448 nm) was quantified by ImageJ software (**c**). Data represent mean ± SD ($n = 3$, 100 cells from three independent experiments). ****$P < 0.0001$, two-way ANOVA. **d** HeLa/Parkin cells were transfected with siLuc or siSNAP29. Forty-eight hours after transfection, cells were treated with OA for 18 h, and immunoblotting was performed with indicated antibodies. Quantification of normalized TOM20, PHB2 and COX2 (right). Data are presented as mean ± SD ($n = 3$, three independent experiments). ns, no significance, two-way ANOVA. **e**, **f** HeLa cells stably expressing Parkin and mito-Keima were transfected with siLuc or siSNAP29. Forty-eight hours after transfection, cells were treated and analyzed as described in **b** (**e**). Scale bars, 10 μm. The relative ratio of fluorescence intensity (552 nm:448 nm) was quantified by ImageJ software (**f**). Data represent means ± SD ($n = 3$, 100 cells from three independent experiments). **g**, **h** FACS-based mito-Keima assay dot plots of siLuc, siSNAP47 or siSNAP29 HeLa cells expressing Parkin with OA treatment. The percentages of cells within the different regions are indicated (**g**). Cells with a high ratiometric (561 nm:488 nm) were selected, and their proportion was calculated (**h**). Data represent mean ± SD ($n = 3$, three independent experiments). ****$P < 0.0001$, ns, no significance, two-way ANOVA. **i** Wild-type (WT), SNAP47 KO, SNAP29 KO and SNAP47/SNAP29 DKO HeLa/Parkin cells were treated with DMSO or OA for 18 h and immunoblotted with indicated antibodies. Quantification of normalized TOM20, PHB2 and COX2 (right). Data are represented as mean ± SD ($n = 3$, three independent experiments). ****$P < 0.0001$. ns, no significance, two-way ANOVA. **j**, **k** WT and SNAP47 KO HeLa/Parkin cells (five independent clones) (**j**) and one rescued clone (**k**) were treated with DMSO or OA for 18 h. Cells were lysed and immunoblotted with indicated antibodies. Quantification of normalized TOM20, PHB2 and COX2 (right in **j**, **k**). Data are represented as mean ± SD ($n = 3$, three independent experiments). ****$P < 0.0001$. ns, no significance, two-way ANOVA. **l** HeLa cells stably expressing GFP-SNAP47 cells were exposed to hypoxia for 0 h or 24 h, and then stained with antibodies against LC3B and HSP60. Scale bars, 5 μm. **m** WT, SNAP47 KO and Flag-SNAP47 complemented SNAP47 KO HeLa cells were exposed to hypoxia for 0 h or 24 h. Cells were lysed and immunoblotted with indicated antibodies. Quantification of normalized TOM20, PHB2 and COX2 (right). Data are represented as mean ± SD ($n = 3$, three independent experiments). ****$P < 0.0001$. *n*s, no significance, two-way ANOVA.

tested whether this PH domain is involved in SNAP47 targeting to autophagic structures. To this end, we used a series of SNAP47 truncation variants for localization analysis, which indicated that variants harboring the SNAP47 PH domain could still localize to autophagosomes and mitophagosomes, whereas variants lacking the PH domain showed no such localization pattern (Fig. 5d, e; Supplementary information, Fig. S11a), supporting that the PH domain is required for SNAP47 targeting to autophagic structures.

Since PH domains are known to show affinity toward different phosphoinositols, we investigated whether the SNAP47 PH domain can bind phosphoinositols and whether it shows specificity toward specific phosphoinositols. In flotation assays with SNAP47 PH domain purified from *E. coli* and liposomes containing different phosphoinositols, the SNAP47 PH preferentially bound to PI(4,5)P_2, but not other phosphoinositols (Fig. 5f). Further in vitro single-vesicle binding assays (Supplementary information, Fig. S12a, b) confirmed that SNAP47 PH could specifically bind to PI(4,5)P_2 (Fig. 5g, h; Supplementary information, Fig. S12c). In agreement with these results, full-length SNAP47 also showed preferential binding to PI(4,5)P_2 (Fig. 5i–k; Supplementary information, Fig. S12d).

In PIP5K1A, PIP5K1B, or PIP5K1C overexpression cells, a portion of SNAP47 PH domain redistributed to plasma membrane compared to WT cells, further suggesting that SNAP47 PH domain can bind PI(4,5)P_2 in vivo (Supplementary information, Fig. S13a). This PH domain also localized to damaged mitochondria (Fig. 5d; Supplementary information, Fig. S13b), while this localization was almost completely blocked in high-expression OCRL cells, a PI(4,5)P_2 5-phosphatase (Supplementary information, Fig. S13c, d). Notably, in cells with relatively lower OCRL expression, some SNAP47$^+$/LC3$^+$/HSP60$^+$ puncta persisted, however, detailed examination revealed that puncta with high OCRL signal consistently exhibited low SNAP47 signal, while puncta with low or no OCRL signal consistently displayed high SNAP47 signal (Supplementary information, Fig. S13e, f). These suggest that SNAP47 PH domain binds mitophagosomal PI(4,5)P_2.

Structural predictions of the SNAP47 PH domain by AlphaFold (Supplementary information, Fig. S11b) with alignment to similar PH domains identified two potential binding regions for PI(4,5)P_2 (Fig. 5l; Supplementary information, Fig. S11c). Molecular docking simulations with the SNAP47 PH domain and inositol-1,4,5-trisphosphate (IP_3-1,4,5, the headgroup of PI(4,5)P_2) suggest that IP_3-1,4,5 likely resides in region 1, with a binding energy of –4.4 kcal/mol (Fig. 5l). Notably, this binding energy was close to that of IP_3-1,4,5 docking with the ArhGAP9 PH domain (–4.9 kcal/mol, Supplementary information, Fig. S11c), another PH domain previously shown to bind PI(4,5)P_2 through region 1.

We next sought to identify the specific residues in these two binding regions potentially required for SNAP47 recognition of PI(4,5)P_2. Since the top loop connecting the first and second beta-sheet showed potentially high flexibility, and the residues within this loop were not all conserved among different species (Fig. 5l; Supplementary information, Fig. S11d), we designed two SNAP47 PH mutants, one harboring a conversion of a conserved, positively charged residue in region 1 (K77E), and the other carrying triple mutations of positively charged residues in the top loop between region 1 and region 2 (K19E/R20E/R21E) (Fig. 5l). While the K19E/R20E/R21E variant displayed remarkably decreased binding to PI(4,5)P_2, the K77E variant also showed significantly decreased PI(4,5)P_2 binding, but to a lesser extent than the K19E/R20E/R21E variant (Fig. 5f, m, n; Supplementary information, Fig. S12e). These results suggest that these positively charged amino acids in both region 1 and region 2 affect PI(4,5)P_2 binding. Co-immunostaining for either variant and mitochondria in HeLa cells showed that mitophagosomes were labeled by significantly less signal of SNAP47-K19E/R20E/R21E or SNAP47-K77E variant than that of WT SNAP47, suggesting that mutation of these residues inhibit both PI(4,5)P_2 binding and SNAP47 targeting to mitophagosomes (Fig. 5o–q). Taken together, these results suggest that PI(4,5)P_2-binding activity of the SNAP47 PH domain is also involved in SNAP47 recruitment to autophagosomes.

Given that PI(4,5)P_2 presents on many other organelles and co-detection of lipids and proteins on membranes ensures the specific protein targeting,[19] we next sought to identify the protein-binding partners of SNAP47. Since STX17 and ATG8 family proteins are present on autophagic vacuoles, we examined whether these proteins are required for SNAP47 recruitment to autophagic vacuoles. In STX17 KO cells, SNAP47 still colocalized with LC3, while conversely STX17 also retained colocalization with LC3 in SNAP47 KO cells upon the induction of mitophagy (Supplementary information, Fig. S11e, f), suggesting that SNAP47 recruitment to mitophagosomes is independent of STX17 and vice versa.

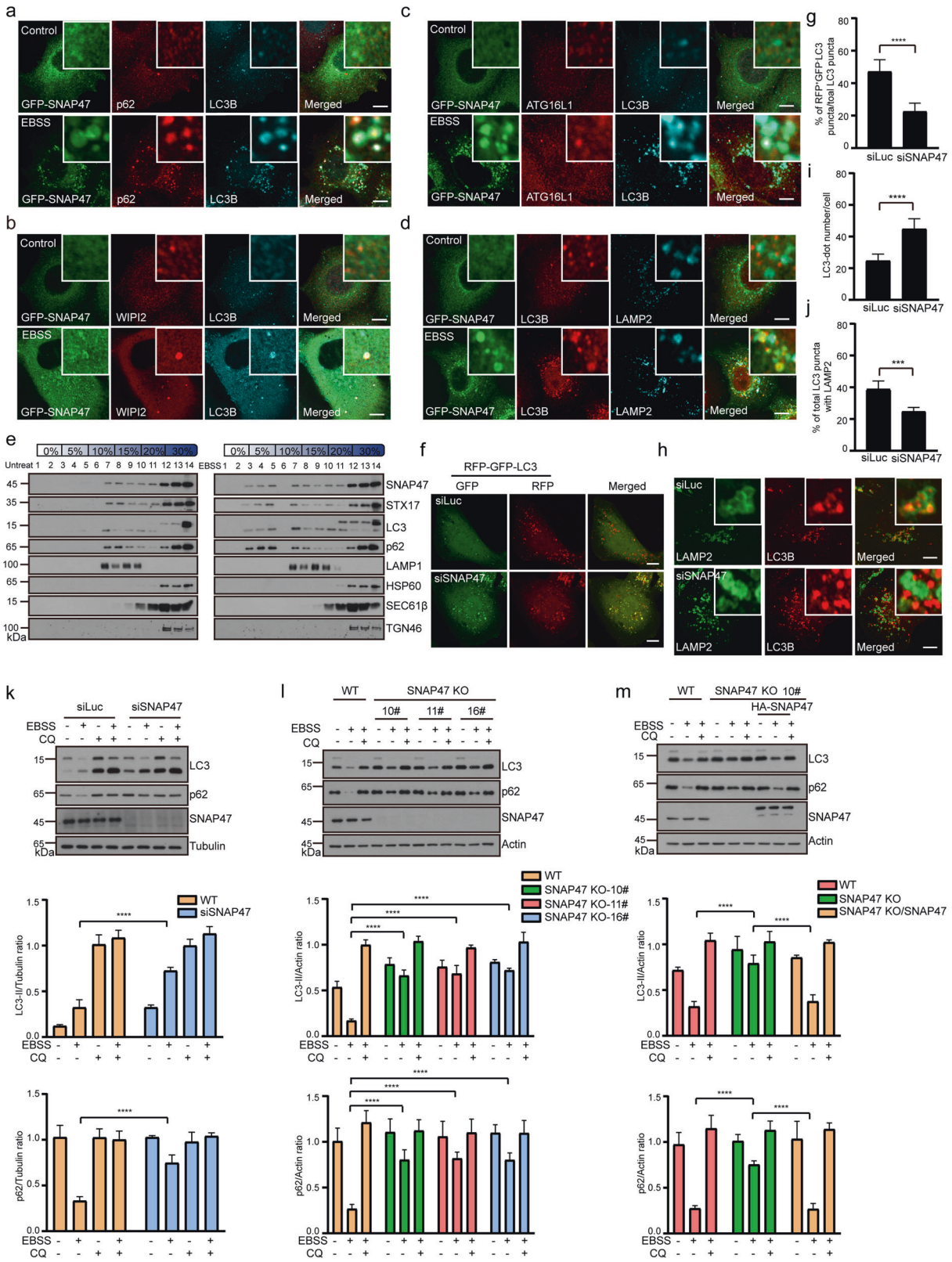

To investigate whether ATG8s participate in SNAP47 mobilization to mitophagosomes, we examined SNAP47 localization in cells knocked out for all six ATG8 proteins (ATG8s KO). Previously, autophagosomes have been found to form in ATG8s KO cells.[20] We found that SNAP47 enclosure of HSP60 was completely abolished in ATG8s KO cells (Fig. 6a), suggesting that ATG8s are required for the recruitment of SNAP47 to mitophagosomes. In order to identify which ATG8 homologues are responsible for SNAP47 recruitment to autophagosomes, ATG8s KO cells were individually complemented with all ATG8 homologues, including

Fig. 3 SNAP47 functions in starvation-induced autophagy. a–d HeLa cells stably expressing GFP-SNAP47 were cultured in regular medium or starvation medium for 2 h and then were stained with indicated antibodies. Scale bars, 5 μm. **e** MEF cells were cultured in regular medium or starvation medium for 2 h, and then cell homogenates were subjected to OptiPrep flotation analysis. **f** U2OS cells stably expressing RFP-GFP-LC3 were treated with siLuc or siSNAP47 for 48 h, then cells were cultured in starvation medium for 2 h (**f**). Scale bars, 5 μm. **g** Quantification of the percentage of RFP^+GFP^- LC3 puncta among total LC3 puncta in **f**. Data are presented as mean ± SD ($n = 3$, 100 cells from three independent experiments). $^{****}P < 0.0001$, unpaired two-tailed *t*-test. **h** U2OS cells were transfected with siLuc or siSNAP47 for 48 h, then cells were cultured in starvation medium for 2 h, and then stained with indicated antibodies. Scale bars, 5 μm. **i** Quantification of the number of LC3 punctate structures per cell in **h**. Data are presented as mean ± SD ($n = 3$, 50 cells from three independent experiments). $^{****}P < 0.0001$, unpaired two-tailed *t*-test. **j** Quantification of the colocalization between LC3 and LAMP2 in **h**. Data are presented as mean ± SD ($n = 3$, 50 cells from three independent experiments). $^{***}P < 0.001$, unpaired two-tailed *t*-test. **k** U2OS cells were transfected with siLuc or siSNAP47 for 48 h, then cells were cultured in regular or starvation medium for 2 h with or without 20 μM CQ (chloroquine) and analyzed by immunoblotting. The intensity of LC3-II and p62 bands was normalized to actin. Data are mean ± SD of three independent experiments. $^{****}P < 0.0001$, two-way ANOVA. **l**, **m** WT and SNAP47 KO HeLa cells (three independent clones) (**l**) and one rescued clone (**m**) were cultured in regular or starvation medium for 2 h with or without 20 μM CQ. Cells were lysed and immunoblotted with indicated antibodies. The intensity of LC3-II and p62 bands was normalized to actin. Data are mean ± SD of three independent experiments. $^{****}P < 0.0001$, two-way ANOVA.

LC3A, LC3B, LC3C, GABARAP, GABARAPL1 and GABARAPL2. We found that LC3A, LC3B, and GABARAP expression could restore SNAP47 enclosure of HSP60, and resulted in a higher efficiency of such activity than rescue of SNAP47 localization by LC3C, GABARAPL1 and GABARAPL2 (Fig. 6b–d), indicating that ATG8s are required for SNAP47 recruitment.

We further speculated that ATG8s may interact with SNAP47 to recruit it to autophagosomes. In support of this hypothesis, we observed that SNAP47, but not SNAP29, directly interacted with all ATG8 homologues (Fig. 6e, f). Importantly, we also identified two potential LIR motifs (LC3-interaction region) at the N terminal of SNAP47 (Fig. 6g). Targeted mutation of the LIR1, LIR2 and LIR1/2 motifs in SNAP47 resulted in remarkably reduced interactions between SNAP47 and ATG8s (Fig. 6h–k), and complete loss of SNAP47 localization to LC3B puncta (Fig. 6l). In addition, SNAP47 LIR1/2 mutants displayed remarkable inhibition of mitochondrial protein degradation (Fig. 6m). In addition, SNAP47 LIR1/2 mutants had no effect on STX17-SNAP47-VAMP7/VAMP8 SNARE complex assembly (Fig. 6n). Taken together, these results suggest that ATG8s participate in recruiting SNAP47 to mitophagosomes via interactions with the SNAP47 LIR motifs.

SNAP29 O-GlcNAcylation contributes to excluding SNAP29 from mitophagosomes

We next investigated how mitophagosomes selectively recruit SNAP47, but not SNAP29, during mitophagy. A previous study reported that SNAP29 O-GlcNAcylation inhibits the autophagosomal localization of SNAP29, assembly of the STX17-SNAP29-VAMP8 complex, and subsequent autophagosome–lysosome fusion.[21] In addition, SNAP29 O-GlcNAcylation was previously shown to decrease during starvation-induced autophagy, promoting autophagosome–lysosome fusion.[21] However, we found that SNAP29 O-GlcNAcylation only decreased in starvation-induced bulk autophagy, but not in autophagy induced by other various stress stimuli **(**Fig. 7a**)**. Furthermore, SNAP47 O-GlcNAcylation could not be detected **(**Fig. 7b**)**. The finding that SNAP29 O-GlcNAcylation was apparently unaffected upon selective autophagy stimuli suggests the possibility that SNAP29 inactivation by O-GlcNAcylation could preclude its participation in SNARE complex assembly and subsequent autophagosome–lysosome fusion in selective autophagy.

Supporting this hypothesis, the formation of STX17-SNAP47-VAMP7/VAMP8 complex increased following the induction of mitophagy, whereas STX17-SNAP29-VAMP8 complex formation remained almost unchanged (Fig. 7c). Moreover, the mitophagosomal localization of SNAP29 QM (an O-GlcNAcylation-deficient mutant[21]) was partially rescued in SNAP47/SNAP29 double KO cells (Fig. 7d), unlike SNAP29 WT. This partial rescue was also observed in mitochondrial protein degradation by SNAP29 QM but not by SNAP29 WT in SNAP47/SNAP29 DKO cells (Fig. 7e). These findings collectively lead us to the conclusion that SNAP29 O-GlcNAcylation results in the exclusion of SNAP29 from autophagosomes during mitophagy.

In addition, though overexpression of STX17 rescued the co-localization of SNAP29 with HSP60 (Fig. 7f), it failed to rescue mitochondrial protein degradation in SNAP47 KO cells (Fig. 7g). It is likely that although STX17 overexpression leads to autophagosomal recruitment of SNAP29, SNAP29 is inactive due to its O-GlcNAcylation. SNAP29 O-GlcNAcylation inhibits STX17-SNAP29-VAMP8 assembly, blocking subsequent autophagosome–lysosome fusion, and SNAP29 O-GlcNAcylation only decreases to promote autophagosome–lysosome fusion during starvation-induced autophagy.[21] However, SNAP29 O-GlcNAcylation does not decrease in mitophagy (Fig. 7a). Therefore, although SNAP29 is recruited to mitophagosomes upon high expression of STX17, the O-GlcNAcylation of SNAP29 still precludes its participation in SNARE complexes and autophagosome–lysosome fusion.

DISCUSSION

In this study, we found that Qbc-SNARE SNAP47 is recruited to autophagosomes and forms the default ternary SNARE complex STX17-SNAP47-VAMP7/VAMP8 to mediate autophagosome–lysosome fusion in both selective autophagy under non-starvation conditions and starvation-induced bulk autophagy. However, SNAP29-containing SNARE complex only functions in starvation-induced autophagy. In this process, the interaction of SNAP47 with $PI(4,5)P_2$ and ATG8s initiates its recruitment to autophagic vacuoles at phagophore stages. SNAP29 is excluded from selective autophagy under non-starvation conditions through its O-GlcNAcylation, while SNAP47 binds autophagosomal STX17 and lysosomal VAMP7/VAMP8 to mediate autophagosome–lysosome fusion under non-starvation conditions. Collectively, our discovery reveals a previously unidentified default SNARE complex that is required for autophagosome–lysosome fusion in starvation-induced bulk autophagy and selective autophagy under non-starvation conditions.

Notably, SNAP47 is the first SNARE protein with a lipid-binding domain identified in mammals. Our findings demonstrate that SNAP47 PH domain mediates its binding with $PI(4,5)P_2$, which is required for SNAP47 recruitment to autophagic vacuoles. Several mechanisms of SNARE protein recruitment to their respective target membranes have been described in mammals.[6] For instance, SNARE complexes with single transmembrane proteins are translocated to the target membranes via vesicle trafficking, while some SNAREs are recruited to specific membranes via hydrophobic membrane anchoring (e.g., SNAP25 or YKT6) or protein–protein interactions. SNAP47 recruitment to autophagic vacuoles via PH domain binding to $PI(4,5)P_2$ thus represents a new mechanism for SNARE targeting in mammals.

In this study, we found that SNAP29 only functions in starvation-induced autophagy, while SNAP47 functions in both bulk and selective autophagy. The simultaneous reduction in

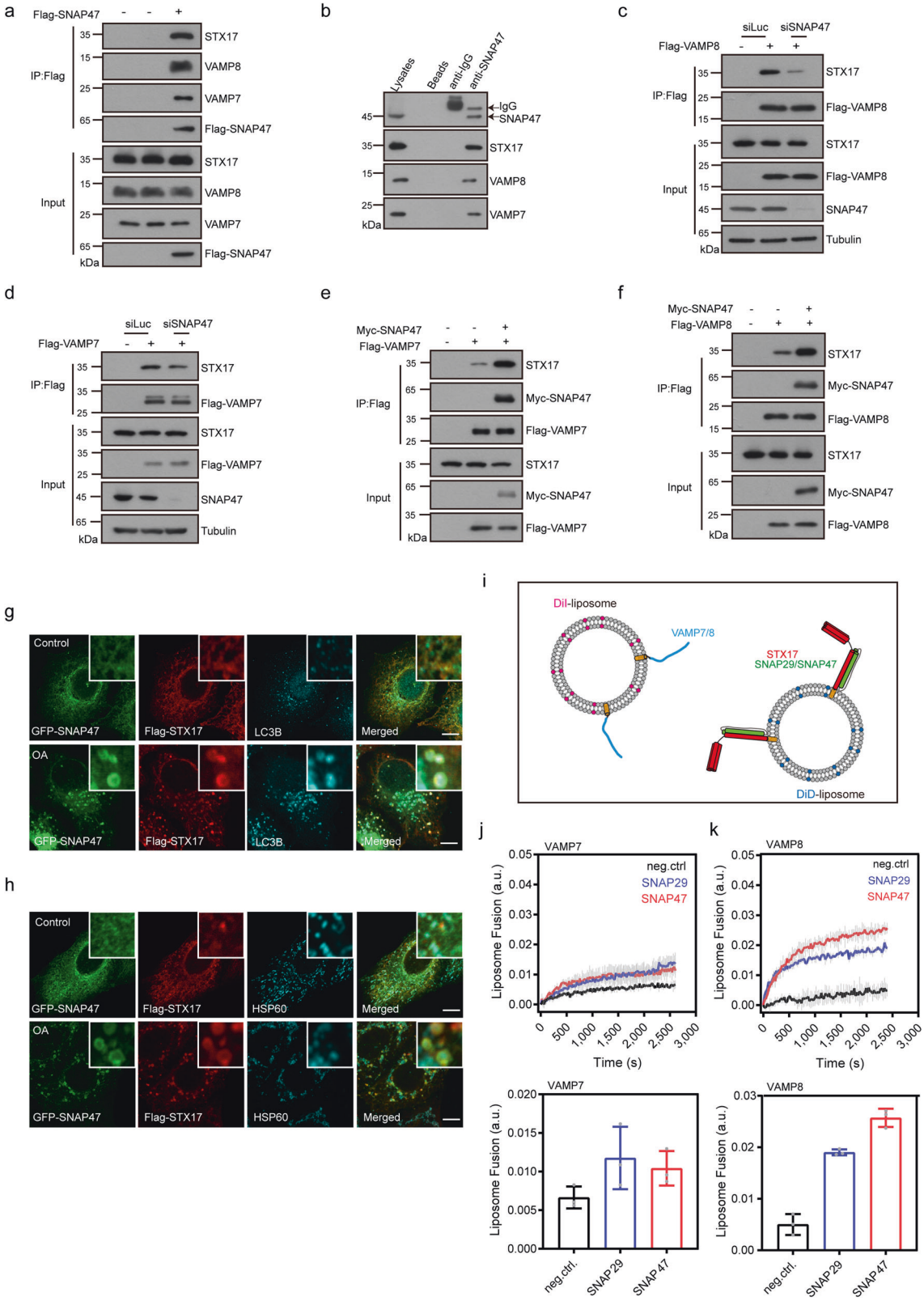

SNAP29 O-GlcNAcylation levels and UDP-GlcNAc has only been reported in EBSS-treated or glucose-starved mammalian cells as well as starved *C. elegans*.[21] Furthermore, SNAP29 O-GlcNAcylation levels can affect starvation-induced bulk autophagy activity by regulating autophagosome–lysosome fusion.[21] These collective findings suggest the possibility that the STX17-SNAP47-VMAP7 and VAMP8 SNARE complex probably participates in the large majority of autophagy during physiological or non-stress conditions, in which the glycosylation status is unchanged, whereas SNARE complexes with SNAP29 are induced during glycosylation-

Fig. 4 SNAP47 forms a ternary SNARE complex with STX17 and VAMP7/VAMP8. a HEK293T cells were transfected with empty vector and Flag-SNAP47. Twenty-four hours after transfection, cells lysates were immunoprecipitated with anti-Flag antibody. **b** HEK293T cells were lysed and immunoprecipitated with anti-SNAP47 antibody. **c** HEK293T cells were transfected with siLuc or siSNAP47. Twenty-four hours after transfection, cells were transfected with empty vector or Flag-VAMP8 for another 24 h. Cell lysates were immunoprecipitated with anti-Flag antibody. **d** HEK293T cells were transfected with siLuc or siSNAP47. Twenty-four hours after transfection, cells were transfected with empty vector or Flag-VAMP7 for another 24 h. Cell lysates were immunoprecipitated with anti-Flag antibody. **e** HEK293T cells were transfected with empty vector, Flag-VAMP7 with or without Myc-SNAP47 for 24 h. Then cell lysates were immunoprecipitated with anti-Flag antibody. **f** HEK293T cells were transfected with empty vector, Flag-VAMP8 with or without Myc-SNAP47 for 24 h. Cell lysates were immunoprecipitated with anti-Flag antibody. **g**, **h** HeLa cells stably expressing Parkin were transfected with GFP-SNAP47 and Flag-STX17. Twenty-four hours after transfection, cells were treated with OA for 4 h, and then were stained with indicated antibodies. Scale bars, 5 μm. **i** Schematic for the experimental procedures used in the reconstituted fusion reactions. Liposomes were reconstituted with the indicated SNAREs to mimic autophagosome–lysosome fusion in vitro. **j, k** Fusion activity between proteoliposomes reconstituted with STX17 and VAMP7 (**j**) or STX17 and VAMP8 (**k**). neg. ctrl denotes no addition of SNAP29 or SNAP47. Each trace was independently repeated three times. The gray bars indicate standard deviations (SD) of each data point. Statistics of the liposome fusion at 2400 s are shown. Data are presented as mean ± SD ($n = 3$ technical replicates).

related metabolic alterations, such as EBSS treatment or glucose starvation. It is plausible that activating SNAP29 may increase the rate of autophagosome–lysosome fusion to alleviate starvation-induced stress when a large amount of autophagosomes are formed in bulk autophagy in a short period of time.

Multiple PIs have been shown to participate in autophagosome–lysosome fusion.[22–32] Among them, the autophagosomal PI(4,5)P_2 functions in both autophagosome formation and autophagosome–lysosome fusion.[28,29,33] In autophagosome formation, PI(4,5)P_2 regulates membrane delivery and ATG14 complex assembly.[28,29] However, the mechanism underlying autophagosomal PI(4,5)P_2 function in autophagosome–lysosome fusion has remained unknown. Here, we identified SNAP47 as an effector of autophagosomal PI(4,5)P_2, and their interaction results in SNAP47 recruitment to autophagosomes to mediate the autophagosome–lysosome fusion. In addition, it is known that ATG14 binds PI(4,5)P_2[29,30] and also regulates autophagosome–lysosome fusion.[9] This also raises a possibility that ATG14 may function together with SNAP47 in the microdomains containing PI(4,5)P_2 on the autophagosome outer membrane.

Mammalian ATG8 family proteins (mATG8s) are well known to contribute to autophagosome formation, cargo recognition, and autophagosome–lysosome fusion by interacting with various components of the autophagy apparatus, highlighting their various and complex roles in autophagy.[22,34–38] An earlier study reported that GABARAPL2/GATE-16 interacts with NSF and GOS-28 to regulate intra-Golgi transport.[39] Recently, mATG8s were shown to bind multiple LIR motif-containing SNAREs.[37] For instance, ATG8s interact with STX17 and STX16 to regulate autophagosomal recruitment of STX17 and endolysosomal localization of STX16, respectively.[37,38,40] Furthermore, it has been reported that the LIR motif is also present in VAMP7 but absent in VAMP8.[37] Here, we found that ATG8s can all interact with the LIR motifs in the PH domain of SNAP47 and direct SNAP47 to autophagosomes. These findings might suggest a potential common regulatory mode of ATG8s in the vesicle fusion process through interactions with SNAREs.

Autophagosome–lysosome fusion involves multiple processes or stages, including SNARE recruitment, vesicle tethering, SNARE assembly, and final vesicle fusion. A previous study reported that the GABARAP subfamily proteins serve as the major regulators for autophagosome–lysosome fusion, whereas the LC3 subfamily proteins contribute to a less extent in this process.[20] Other groups found that EPG5, PLEKHM1, BRUCE, and GRASP55 interact with ATG8s for vesicle tethering in autophagosome–lysosome fusion.[41–43] These findings suggest that ATG8s likely contribute to different stages of autophagosome–lysosome fusion. Despite the lower efficiency of SNAP47 recruitment by GABARAPL1 and GABARAPL2, the amount of SNAP47 may be sufficient to mediate subsequent autophagosome–lysosome fusion. Moreover, while LC3A and LC3B recruit SNAP47 more efficiently, autophagosome–lysosome fusion can also be blocked in later stages due to lack of GABARAPs. This could explain why SNAP47 targeting is rescued with higher efficiency by LC3A and LC3B in GABARAPs deficient cells, but mitophagy is still defective.

It should also be noted that PI(4,5)P_2 and ATG8s are both required for SNAP47 localization to autophagic structures, and that SNAP47 localization to autophagic structures will fail in the absence of either. These findings are consistent with the coincidence detection model that has been proposed for many other membrane-binding proteins.[19] ATG8s and PI(4,5)P_2 are also found separately on other organelles, and thus their co-detection could potentially specify SNAP47 localization to autophagic structures.

During autophagosome maturation, many events occur in a time-dependent manner.[44] SNAP47 is recruited to autophagic vacuoles during the phagophore stage, whereas the other autophagosomal SNARE, STX17, is exclusively recruited to fully sealed autophagosomes, as demonstrated in a prior study.[7,45] Consequently, it is plausible that SNAP47's recruitment to phagophores, which lack STX17, and the delayed recruitment of STX17 to sealed autophagosomes, help prevent SNAP47-STX17 interactions during the phagophore stage. This temporal separation likely serves to inhibit premature fusion of phagophores with lysosomes.

Although SNAP47 depletion significantly hinders the degradation of mitochondrial proteins, it does not fully restore the mitochondrial protein levels to baseline. It is plausible that alternative pathways exist for mitochondria clearance. Recent research has indicated that damaged mitochondria in OA-induced mitophagy can be secreted from the cell independently of the mATG8-conjugation machinery.[46] Moreover, mitochondria can also be released through processes such as mitocytosis,[47] mitolysosome exocytosis,[48] or impaired lysosomes.[49] These pathways mentioned above could collectively contribute to the incomplete restore of mitochondria protein levels in cells with SNAP47 depletion.

SNAP29 and SNAP47 both belong to the Qbc-SNARE subfamily. However, there are several noteworthy differences between them. First, the additional PH domain in SNAP47 is a structurally important feature beyond that of their shared Qbc-SNARE domain. Second, SNAP47 is recruited to autophagic vacuoles earlier via binding with PI(4,5)P_2 and ATG8s beginning in the phagophore stage. Third, SNAP29 is regulated by O-GlcNAcylation while SNAP47 is not. Finally, SNAP47 does not interact with YKT6, suggesting that SNAP47 cannot replace SNAP29 in the YKT6-SNAP29-STX7 SNARE complex. These cumulative differences result in SNAP29 participating in starvation-induced bulk autophagy through the STX17-SNAP29-VAMP7/VAMP8 and YKT6-SNAP29-STX7 SNARE complexes, while SNAP47 contributes to both starvation-induced bulk autophagy and selective autophagy under non-starvation conditions through activity of the STX17-SNAP47-VAMP7/VAMP8 SNARE complex.

In addition, we have identified a preference for SNAP47 to interact with VAMP4, VAMP5, VAMP7, VAMP8, STX1B, and STX4.

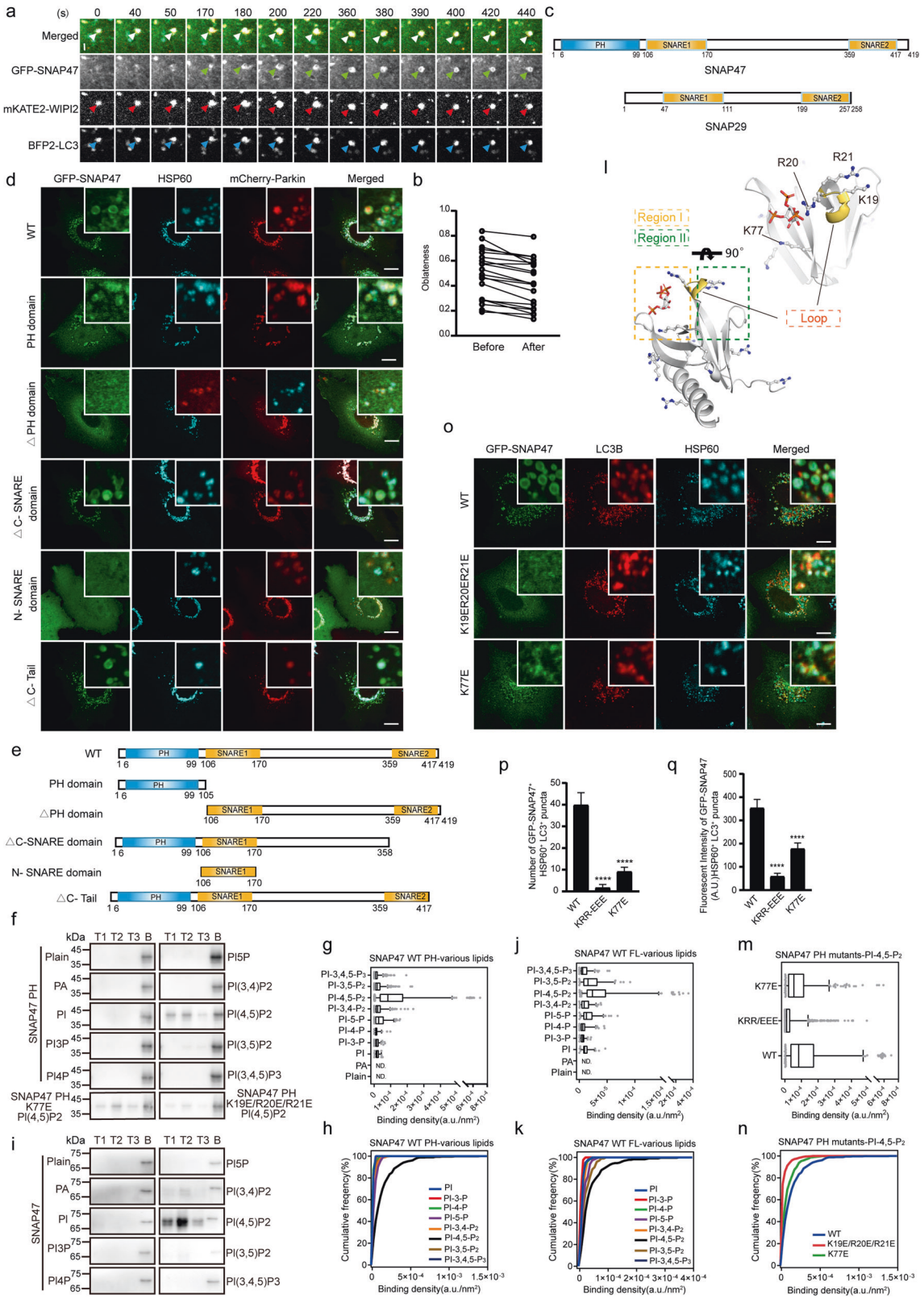

This observation is consistent with previous research findings,[50,51] which have reported the interaction of SNAP47 with VAMP7 and VAMP8, and their interaction play a role in the proper localization and function of a subset of VAMP proteins.[50] Furthermore, SNAP47 has been shown to cooperate with VAMP5, STX1B, and STX4, contributing to the regulation of exocytosis.[51] In our study, we have provided new evidence demonstrating that SNAP47 is involved in the fusion of autophagosomes with lysosomes, achieved through its cooperation with VAMP7 and VAMP8.

Fig. 5 The binding between PH domain of SNAP47 and PI(4,5)P2 is required for SNAP47 recruitment to autophagic vacuoles. **a**, **b** HeLa/Parkin cells stably expressing GFP-SNAP47, mKATE2-WIPI2 and BFP2-LC3 were treated with OA, and the movie was taken (**a**). Scale bars, 1 μm. The oblateness of LC3 and WIPI2-positive structures before and after appearance of SNAP47 signals ($n = 20$) was quantified (**b**). **c** The schematic diagram of SNAP47 and SNAP29. **d** HeLa cells stably expressing mCherry-Parkin were transfected with GFP-SNAP47 truncated variants. Twenty-four hours after transfection, cells were treated with DMSO or OA for 4 h, and then stained with anti-HSP60 antibody. Scale bars, 5 μm. **e** The Schematic diagram of SNAP47 truncated variants. **f** Binding of SNAP47-PH WT or mutants to different phosphatidylinositols (PIs) was analyzed by liposome floatation assays. **g**, **h** Binding densities of SNAP47-PH to different PIs were analyzed by single-vesicle binding assays. Data are presented by box-whisker graphs with outliers (out of 5%–95% percentile) shown by gray scatters. Plain (POPC and POPE only) and PA (phosphatidic acid) were not analyzed since the binding densities were below the threshold (**g**). Cumulative frequencies of the binding density data in **g** are shown (**h**). **i** Binding of SNAP47 full-length to different PIs was analyzed by liposome floatation assays. **j**, **k** Binding densities of SNAP47 full-length to different PIs was analyzed by single-vesicle binding assays. Data are presented by box-whisker graphs with outliers (out of 5%–95% percentile) shown by gray scatters. Plain (POPC and POPE only) and PA (phosphatidic acid) were not analyzed since the binding densities were below the threshold (**j**). Cumulative frequencies of the binding density data in **j** are shown (**k**). **l** Molecular docking of IP3-1,4,5 (PI-4,5-P2 headgroup) to predict structure of SNAP47-PH. Positively-charged residues (Lys, Arg, and His) are shown by ball-and-stick model. The optimal docking model shown in the graph gives a binding energy (ΔG) of −4.4 kcal/mol. The PIs-binding pockets are indicated by green and orange dashed boxes. **m**, **n** Binding densities of SNAP47-PH WT or mutants (K19E/R20E/R21E, K77E) to PI(4,5)P2-containing liposomes was analyzed by single-vesicle binding assays. Data are presented by box-whisker graphs with outliers (out of 5%–95% percentile) shown by gray scatters (**m**). Cumulative frequencies of the binding density data in **m** are shown (**n**). **o** HeLa/Parkin cells stably expressing WT or mutants (K19E/R20E/R21E and K77E) GFP-SNAP47 were treated with DMSO or OA for 4 h. Cells were then stained with indicated antibodies. Scale bars, 5 μm. **p** Quantification of the number of GFP-SNAP47$^+$LC3$^+$HSP60$^+$ puncta. Images in **o** were analyzed. Data are mean ± SD ($n = 3$, 100 cells from three independent experiments were quantified). ****$P < 0.0001$, one-way ANOVA. **q** Quantification of the mean fluorescent intensity of SNAP47 on mitophagosome in **o**. Data are mean ± SD ($n = 3$, 300 autophagosomes from three independent experiments were quantified). ****$P < 0.0001$, one-way ANOVA.

In vitro fusion assays showed that the STX17-SNAP47-VAMP7 SNARE complex exerts less fusogenic activity than the STX17-SNAP47-VAMP8 SNARE complex. This lower fusogenic activity may be attributable to inhibitory effects of the SNARE N-terminal domain, as described in previous reports.[52] In particular, VAMP7 has an N-terminal longin domain preceding the SNARE domain, which is absent in VAMP8. It is likely that this Longin domain may have an autoinhibitory effect on the fusogenic activity of the STX17-SNAP47-VAMP7 SNARE complex in vitro, since the effect of the Longin domain in VAMP7 or Ykt6 negatively regulates SNARE complex function via intramolecular binding to the SNARE domain in a manner reminiscent of syntaxins.[53–56] It is conceivable that VAMP7 may require additional factors to fulfill its function in vivo, which are absent in our in vitro system.

Autophagosome–lysosome fusion is a critical step for fulfilling autophagic function. In this study, we identified a previously unreported default SNARE complex (STX17-SNAP47-VAMP7/VAMP8) involved in starvation-induced autophagy and selective autophagy under non-starvations. Further study is warranted to determine whether any accessory mechanisms or upstream regulators participate in autophagosome–lysosome fusion process. In addition, since many types of autophagy have been implicated in multiple human diseases, our findings provide a common mechanistic basis for developing targeted therapeutic interventions for diseases related to dysfunction of autophagy.

MATERIALS AND METHODS

Cell culture and transfection

HEK293T, U2OS, MEF, COS7, HepG2 and HeLa cells were cultured in DMEM (Hyclone) supplemented with 10% FBS (Gibco) and 1% Penicillin-Streptomycin Solution (Beyotime) at 37 °C with 5% CO_2. For starvation treatment, cells were washed three times with PBS (Hyclone) and then incubated with EBSS for the indicated time. HeLa cells were transiently transfected using Lipofectamine 3000 (Invitrogen) according to the manufacturer's instructions. Transient transfection of plasmid in HEK293T cells was performed using PEI according to the manufacturer's protocol. The stealth RNAi oligonucleotides were transfected into cells using Lipofectamine RNAiMAX (Invitrogen) according to the manufacturer's instructions. 2 d after transfection, cells were harvested for analysis.

The information of reagents, antibodies, siRNA sequences and lipids used in this study was included in Supplementary Materials.

Immunostaining assay

Cells grown on coverslips were washed with PBS and fixed in 4% paraformaldehyde in PBS for 15 min at room temperature. After washing three times with PBS, cells were permeabilized with 0.1% saponin in PBS for 10 min and then blocked with 10% FBS in PBS for 1 h. Cells were then incubated with primary antibodies for 1 h or overnight at 4 °C. After washed three times with PBS, cells were incubated with the appropriate secondary antibodies at room temperature for 1 h, and washed three times with PBS. The slides were mounted and images were acquired under a laser scanning confocal microscope (FV3000, Olympus).

Mito-Keima mitophagy assay

HeLa cells stably expressing Parkin were infected with a lentivirus carrying the mito-Keima vector. Subsequently, these cells were transfected with the indicated siRNA duplexes for 48 h. Following this, the cells were treated with or without OA in fresh growth medium for 18 h, and were then analyzed using confocal microscopy or FACS.

Live cells were cultured in glass-bottom dishes. After OA treatment, the cells were scanned, and images were acquired using a laser scanning confocal microscope (FV3000, Olympus) with argon lasers (at 448 nm for mito-Keima at neutral pH and 552 nm for mito-Keima at acidic pH). Ratiometric analysis (552 nm:448 nm) was performed using ImageJ software.

For the FACS-based mito-Keima assay, cells were trypsinized, washed once with PBS, and then resuspended in sorting buffer (containing 145 mM NaCl, 5 mM KCl, 1.8 mM $CaCl_2$, 0.8 mM $MgCl_2$, 10 mM HEPES, 10 mM Glucose, 0.1% BSA). The cells were then analyzed using a SONY ID7000 flow cytometry machine. Lysosomal mito-Keima measurements were obtained via dual-excitation ratiometric pH measurements, with lasers at 488 nm (pH 7) and 561 nm (pH 4), and emission filters of 620/29 nm and 614/20 nm, respectively. For each sample, 30,000 events were collected, and data analysis was carried out using FlowJo software (Tree Star, San Carlos, USA).

Immunoprecipitation assay

HEK293T cells were washed in ice-cold PBS and lysed in lysis buffer (20 mM Tris-HCl, pH 7.5, 150 mM NaCl, 1 mM EDTA, 0.5% NP-40, 1 μg/mL Aprotinin, 1 μg/mL Pepstatin A, 1 μg/mL Leupeptin, 200 mM NaF, 200 mM Na_3VO_3) for 30 min at 4 °C. After centrifugation at 12,000× g for 10 min at 4 °C, the supernatants were subjected to immunoprecipitation using anti-Flag M2 (A2220; Sigma-Aldrich) or anti-HA Affinity Gel (A2095; Sigma-Aldrich) for 12 h at 4 °C. Precipitated immunocomplexes were washed three times in lysis buffer and boiled in 2× sample buffer. Samples were then subjected to SDS-PAGE and analyzed by Western Blotting assay.

Western blotting assay

Cells were harvested and lysed with sodium dodecyl sulphate (SDS) buffer. Samples extracted from cells were subjected to SDS-PAGE electrophoresis and immobilized on a polyvinylidene fluoride (PVDF) membrane (BIO-RAD, 162-0177). After blocked with 5% nonfat milk in PBST, membrane was incubated with the primary antibodies, followed by incubated with HRP-conjugated secondary antibody for 1 h at room temperature.

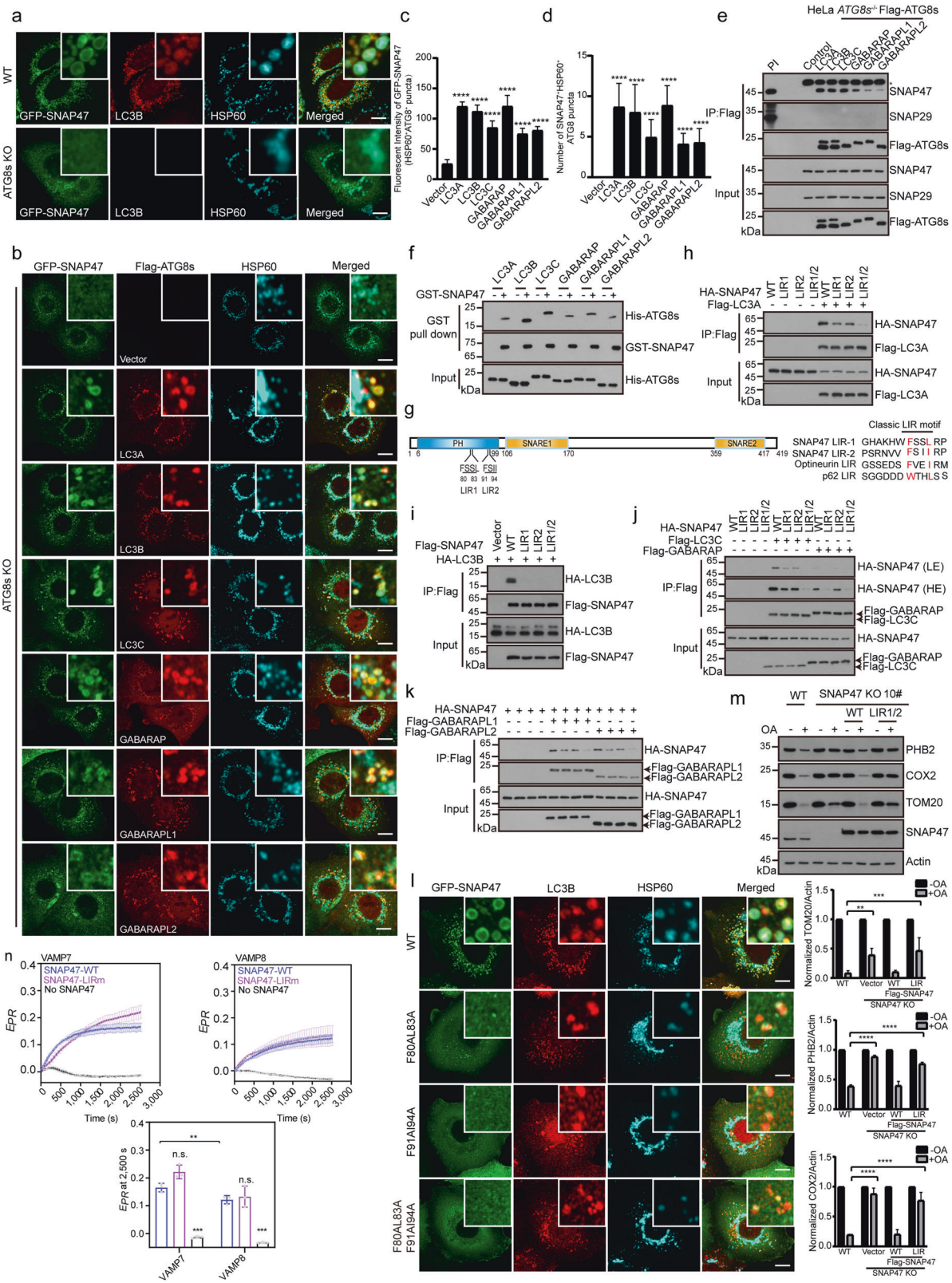

Cell fractionation

Cells from four 10-cm or 15-cm dishes were harvested and washed twice with ice-cold PBS. Cell pellets were collected after centrifugation at 500× *g* for 1 min and resuspended in 1 mL ice-cold homogenization buffer (250 mM sucrose, 20 mM HEPES-KOH, pH 7.4 and complete EDTA-free protease inhibitor) and homogenized in a 2 mL Dounce homogenizer. The homogenized cells were centrifuged twice at 1000× *g* for 10 min to remove cell debris and undisrupted cells. The supernatant was centrifuged at 10,000× *g* for 10 min and then the resultant supernatant was centrifuged at 20,000× *g* for 20 min to collect the pellet. Subsequently, the pellet was diluted in an equal volume of 30% OptiPrep. A discontinuous OptiPrep gradient was generated in centrifuge tubes (Beckman Coulter, 326819) for ultracentrifuge rotors (Beckman Coulter,

Fig. 6 ATG8 family proteins are required for SNAP47 recruitment to autophagic vacuoles. a WT or ATG8s KO (LC3A, LC3B, LC3C, GABARAP, GABARAPL1, GABARAPL2) HeLa cells stably expressing Parkin and GFP-SNAP47 were treated with DMSO or OA for 4 h. Cells were then stained with anti-LC3B and anti-HSP60 antibodies. Scale bars, 5 μm. **b** ATG8s KO HeLa cells stably expressing Parkin and GFP-SNAP47 were transfected with empty vector or individual Flag-ATG8 homologs. Twenty-four hours after transfection, cells were treated with DMSO or OA for 4 h, and then cells were stained with indicated antibodies. Scale bars, 5 μm. **c** Quantification of the mean fluorescent intensity of SNAP47 on mitophagosome in **b**. Data are mean ± SD ($n = 3$, 300 autophagosomes from three independent experiments were quantified). $^{****}P < 0.0001$, one-way ANOVA. **d** Quantification of the number of GFP-SNAP47^{+}LC3^{+}HSP60^{+} puncta. Images in **b** were analyzed. Data are mean ± SD ($n = 3$, 50 cells from three independent experiments were quantified). $^{****}P < 0.0001$, one-way ANOVA. **e** ATG8s KO HeLa cells stably expressing individual Flag-ATG8 homologs were lysed and immunoprecipitated with anti-Flag antibody. PI line is for indicating the position of SNAP47 and SNAP29. **f** Glutathione Sepharose beads bound with GST or GST-SNAP47 were incubated with purified His-tagged LC3A, LC3B, LC3C or GABARAP, GABARAPL1 and GABARAPL2 for 16 h, and then eluted for immunoblotting. **g** Typical LIR sequences were aligned manually alongside SNAP47 for comparison. Red letters indicate highly conserved residues in the putative LIR. **h** HEK293T cells were transfected with WT or LIR mutants (LIR1 F80AL83A, LIR2 F91AI94A, LIR1/2 F80AL83A&F91AI94A) of HA-SNAP47 with or without Flag-LC3A. Twenty-four hours after transfection, cells lysates were immunoprecipitated with anti-Flag antibody. **i** ATG8s KO HeLa cells stably expressing HA-LC3B with or without WT or LIR mutants of Flag-SNAP47 were lysed and immunoprecipitated with anti-Flag antibody. **j** HEK293T cells were transfected with WT or LIR mutants of HA-SNAP47 with or without Flag-LC3C or Flag-GABARAP. Twenty-four hours after transfection, cells lysates were immunoprecipitated with anti-Flag antibody. LE, light exposure; HE, high exposure. **k** HEK293T cells were transfected with WT or LIR mutants of HA-SNAP47 with or without Flag-GABARAPL1 or Flag-GABARAPL2. Twenty-four hours after transfection, cells lysates were immunoprecipitated with anti-Flag antibody. **l** HeLa/Parkin cells stably expressing WT or LIR mutants of GFP-SNAP47 were treated with DMSO or OA for 4 h. Cells were then stained with indicated antibodies. Scale bars, 5 μm. **m** WT, SNAP47 KO, and Flag-SNAP47 WT or Flag-SNAP47 LIR1/2 mutant complemented SNAP47 KO HeLa/Parkin cells were treated with or without OA. Immunoblotting was performed with indicated antibodies. Quantification of normalized TOM20, PHB2 and COX2 in **m**. Data are represented as mean ± SD ($n = 3$, three independent experiments). $^{****}P < 0.0001$, two-way ANOVA. **n** Assembly of the SNARE complex containing STX17, SNAP47 (WT and LIR mutant), and VAMP7/VAMP8 was analyzed by FRET assays. Each trace was independently repeated for three times. The bars indicate SD of each data point. Statistics of EPR (relative proximity ratio of FRET) at 2500 s are shown. Data are presented as means ± SD. $n = 3$ technical replicates. $^{**}P < 0.01$, $^{***}P < 0.001$, two-way ANOVA.

MLS 50) by overlaying the following OptiPrep solutions all in homogenization buffer: 982 μL of the supernatant in 30% OptiPrep (sample), 738 μL 20% OptiPrep, 820 μL 15% OptiPrep, 820 μL 10% OptiPrep, 820 μL 5% OptiPrep and 820 μL 0% OptiPrep. The gradient was centrifuged at 150,000× *g* using ultracentrifuge for 5 h and ultimately 14 fractions (350 μL each) were collected from the top.

Correlative Light and Electron Microscopy (CLEM)

For CLEM, HeLa/Parkin expressing GFP-SNAP47 and mKATE2-WIPI2 were seeded in a gridded glass bottom dish (Cellvis, D35-14-1.5GI) for 24 h. The cells were fixed with 4% PFA for 20 min at room temperature. Fluorescence images were captured by Olympus FV3000 confocal microscope. The cell shape and the position of ROI (Region of Interest) were acquired and recorded under bright field. After imaging, the cells were fixed with 2.5% glutaraldehyde for 1 h at room temperature, and washed 3 times for 5 min each with 0.1 M PB buffer. Then, the samples were post-fixed in 1% OsO4 for 30 min on ice. Cells were washed 3 times for 5 min each with ultrapure water, and then placed in 1% aqueous uranyl acetate for 1 h. Afterward, samples were then washed 3 times for 5 min each with ultrapure water, and dehydrated in a cold-graded ethanol series (50%, 70%, 80%, 90%, 100%, 100%, 100%; 2 min in each). Penetrating in EPON 812 resin using 1:1 (v/v) resin and ethanol for 8 h, 2:1 (v/v) resin and ethanol for 8 h, 3:1 (v/v) resin and ethanol for 8 h, and then pure resin 2 times for 8 h each. Finally, the samples were then placed into fresh resin and polymerisatio-ninoven at 60 °C, for 48 h. The grids were engraved on the resin surface allowing for the location of ROIs on the resin surface. The samples of ROI were cut into 80-nm-thick sections. Stained sections were observed with the H-7650 80kv transmission electron microscope.

In vitro binding assay

Genes were cloned into pGEX-4T-1 or pET-28a vectors for expression in *E. coli* BL21 (DE3). The recombinant proteins were purified by Glutathione-Sepharoseresin 4B (GE healthcare, 17-0756-04) or Ni-NTA affinity resin (Sangon Biotech, C600033). In GST pull-down assays, GST and GST-tagged proteins were applied to GST resin and were then incubated with 1 μg His-tagged proteins in binding buffer (20 mM Tris-HCl, pH 7.4, 150 mM NaCl, 1 mM EDTA, 0.5% NP-40) supplemented with protease inhibitor cocktail (Roche) for 2 h at 4 °C. After three washes, proteins were eluted and dissolved in sample buffer for SDS–PAGE and immunoblotting.

Recombinant protein purification

GST-SNAP47 was expressed in *E. coli* BL21. Bacteria were treated with 0.4 mM IPTG at 16 °C to induce protein expression and were harvested and resuspended in PBS containing 0.5% Triton X-100, 2 mM EDTA, and 1 mM PMSF, followed by ultrasonication. The recombinant SNAP47 proteins were purified using Glutathione-Sepharose 4B beads (GE healthcare, 17-0756-04), eluted with glutathione at 4 °C for 4 h to release the proteins.

Ensemble lipid/content-mixing assays

1-palmitoyl-2-oleoyl-glycero-3-phosphocholine (POPC), 1-palmitoyl-2-oleoyl-sn-glycero-3-phosphoethanolamine (POPE), and 1,2-dioleoyl-sn-glycero-3-phospho-(1′-myo-inositol-3′-phosphate) ammonium salt (PI[3]P) were obtained from Avanti Polar Lipids and dissolved in chloroform at a final concentration of 10 mg/mL except for PI[3]P, which was dissolved in a mixture of chloroform:methanol 2:1 at a concentration of 1 mg/mL. 1,1′-dioctadecyl-3,3,3′,3′-tetramethylindocarbocyanine ($DiIC_{18}$(3)) and 1,1″-dioctadecyl-3,3,3″,3″-tetramethylindodicarbocyanine ($DiDC_{18}$(5)) were obtained from Molecular Probes and dissolved in ethanol at a concentration of 1 mg/mL. Lipids were mixed at the proper ratio as indicated below to a final concentration of 1 mM. Donor liposome (reconstituted with full-length VAMP7 or VAMP8) contains 75.5% POPC, 20% POPE, 3% PI[3]P, and 1.5% DiI (molar ratio). Acceptor liposome (reconstituted with full-length Syntaxin 17) contains 75.5% POPC, 20% POPE, 3% PI[3]P, and 1.5% DiD (molar ratio). Lipid mixtures were dried under nitrogenflow and further incubated in vacuum for 1 h at room temperature in the dark. Lipid films were resuspended in buffer T (20 mM Tris-Cl pH 8.0, 150 mM NaCl) supplied with 0.2 mM Tris (2-Tris (2-carboxyethyl)) phosphine (TCEP, Sigma-Aldrich) and 1% CHAPS (w/v, Amresco). Purified proteins were added to resuspended lipids with a protein-to-lipid ratio of 1:500. After incubation on the ice for 20 min, lipid–protein mixtures were desalted using PD-10 desalting column (GE Healthcare). Prepared proteoliposomes were stored at 4 °C in the dark before use. Liposome fusion assays were carried out using a FluoDia T70 fluorescence plate reader (PTI) equipped with 530/10 excitation filter, 580/10 and 667/10 emission filters at 37 °C. Donor and acceptor liposomes were mixed at a concentration of 100 μM (total lipids) with addition of 2 μM recombinant SNAP29 or SNAP47. Donor (DiI) and acceptor (DiD) fluorescence were monitored every 20 s. Liposome fusion signals were interpreted as the FRET efficiency between the donor (DiI) and acceptor (DiD):

$$E_{FRET} = \frac{I_{DiD}}{I_{DiD} + I_{DiI}}$$

Where the I_{DiD} and I_{DiI} are the fluorescence intensities of DiD and DiI under the 530/10 excitation filter, respectively. All the experiments were independently repeated three times.

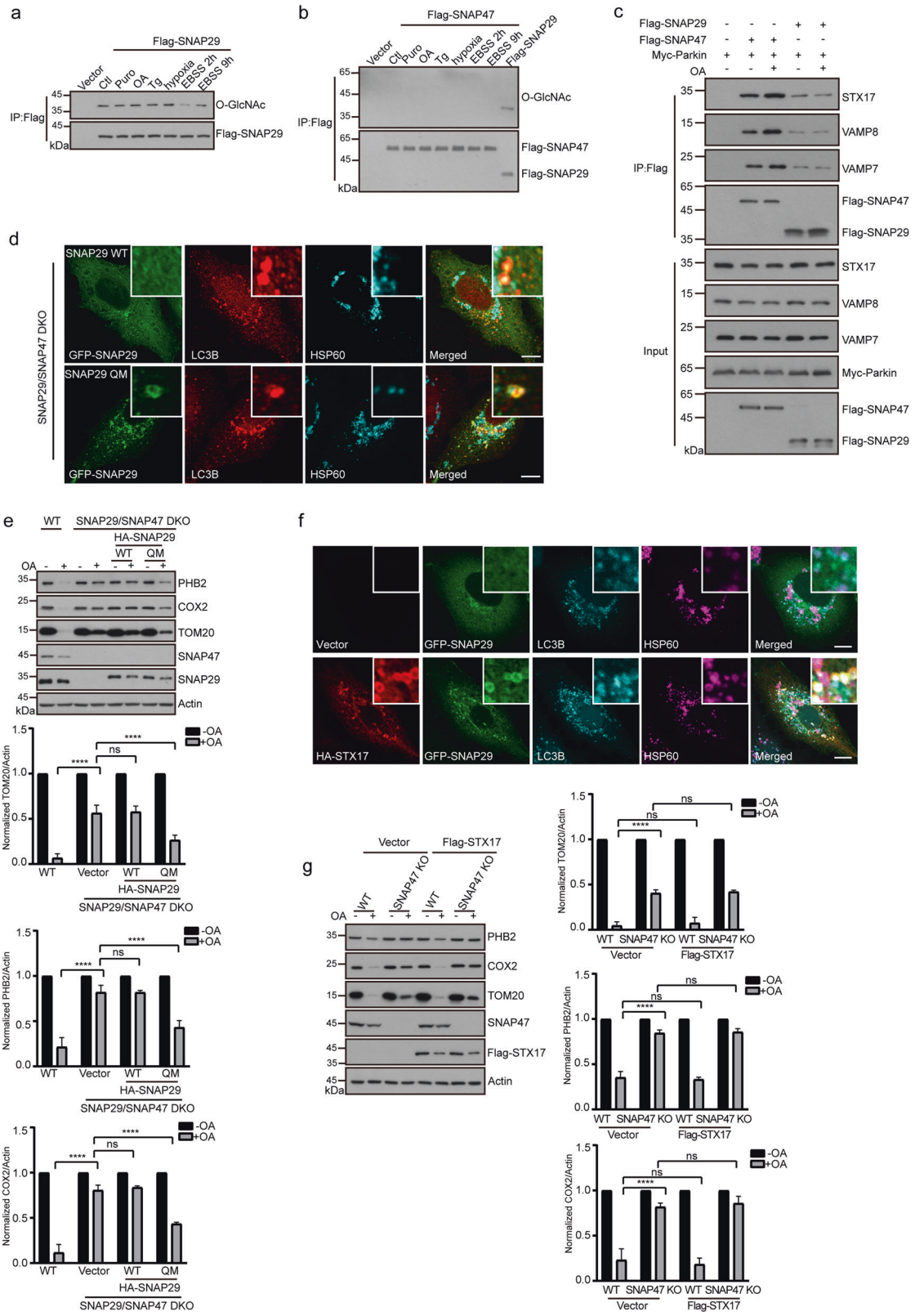

Liposome floatation

Liposomes containing 74.8% POPC, 20% POPE, 5% PIs, and 0.2% DiI (molar ratio) were dried under nitrogen flow and further incubated in vacuum for 1 h at room temperature in the dark. Lipid films were dissolved by freezing and thawing in TBS300 buffer with liquid nitrogen. Dissolved lipids were then extruded through a Whatman 0.8 μm polycarbonate film (Avanti Polar Lipids, #610009) using a mini extruder (Avanti Polar Lipids, #610000). Prepared liposomes were stored at room temperature before used.

500 μM (total lipids) liposomes and 10 μM proteins were first incubate (total 200 μL) at 25 °C for 2 h. The mixtures were then mixed with 200 μL

Fig. 7 SNAP29 O-GlcNAcylation inhibits its recruitment to mitophagosomes. a, **b** HeLa cells stably expressing Flag-SNAP29 (**a**) or Flag-SNAP47 (**b**) were treated with puromycin (10 μg/mL for 4 h), OA (oligomycin 2.5 μM and antimycin-A 250 nM for 4 h), Thapsigargin (Tg 1 μM for 6 h), hypoxia (1% O_2 for 12 h) and EBSS (2 h and 9 h). Cell lysates were immunoprecipitated with anti-Flag antibody. **c** HEK293T stably expressing Myc-Parkin cells were transfected with empty vector, Flag-SNAP47 or Flag-SNAP29. Twenty-four hours after transfection, cells were treated with DMSO or OA for 4 h. Cells were then lysed and immunoprecipitated with anti-Flag antibody. **d** SNAP29/SNAP47 DKO HeLa/Parkin cells stably expressing WT or O-GlcNAcylation mutant (QM: S2A, S61G, T130A, S153G) GFP-SNAP29 were treated with DMSO or OA for 4 h. Cells were then stained with indicated antibodies. Scale bars, 5 μm. **e** WT, SNAP29/SNAP47 DKO and WT or O-GlcNAcylation mutant (QM) of HA-SNAP29 complemented SNAP29/SNAP47 DKO HeLa/Parkin cells were treated with or without OA. Immunoblotting was performed with indicated antibodies. Quantification of normalized TOM20, PHB2 and COX2 (right). Data are represented as mean ± SD ($n = 3$, three independent experiments). ****$P < 0.0001$. ns, no significance, two-way ANOVA. **f** HeLa/Parkin stably expressing GFP-SNAP29 cells were transfected with vector or HA-STX17. Twenty-four hours after transfection, cells were treated with DMSO or OA for 4 h, and then immunostained with indicated antibodies. Scale bars, 5 μm. **g** WT and SNAP47 KO HeLa/Parkin cells stably expressing Flag-STX17 were treated with DMSO or OA for 18 h. Cells were lysed and immunoblotted with indicated antibodies. Quantification of normalized TOM20, PHB2 and COX2 (right). Data are represented as mean ± SD ($n = 3$, three independent experiments). ****$P < 0.0001$. ns, no significance, two-way ANOVA.

80% (w/v) Histodenz (Sigma, #D2158) to produce 40% (w/v) Histodenz cushion. To produce 40%:30%:0% Histodenz discontinuous gradient, another two cushions containing 300 μL 30% (w/v) Histodenz and 10 μL TBS150 were sequentially added. Ultracentrifugation was carried out by using SW55Ti rotor (Beckman Coulter) at 240,000× *g*, 20 °C for 1 h on L-80XP ultracentrifuge (Beckman Coulter). After centrifugation, top 3 fractions (25 μL each, T1, T2, and T3) and bottom fraction (B) were taken and analyzed by SDS-PAGE and western blotting assay with rabbit anti-GST antibody (Proteintech, #10000-0-AP) and HRP-conjugated goat anti-rabbit IgG (Proteintech, #SA00001-2).

Structure prediction by AlphaFold

The protein sequence of human SNAP47 was fetched from UniProt (https://www.uniprot.org/) with entry of A0A087X0B7. Prediction of the 3D structure was achieved by using Colab AlphaFold.ipynb(https://colab.research.google.com/github/deepmind/alphafold/blob/main/notebooks/AlphaFold.ipynb) with AlphaFold v2.3.1.

Molecular docking

The 3D structure of IP_3-1,4,5 was downloaded from PubChem (CID: 136212498). The 3D structure of ARNO (Arf nucleotide binding site opener)-PH (pdb entry: 1u29) and ArhGAP9 (Rho-type GTPase-activating protein 9)-PH (pdb entry: 2p0d) were fetch from RCSB PDB (https://www.rcsb.org/). The structures were preprocessed by AutoDockTools (v1.5.6) to remove waters, ions, non-polar hydrogens, non-bonded ligands and apply torsions. In this paper, the torsions were only applied to ligand (i.e., IP_3-1,4,5) and the proteins were set as rigid conformers. The searching grid box was constrained to the regions I and II for IPs binding. Docking of IP_3-1,4,5 to PH domains were achieved by using Autodock Vina (v1.1.2). The results were manually checked. Those below the binding energy cutoff (−3.0 kcal/mol) or beyond the region I and II were not considered. The optimal docking model for each docking session that possess largest binding energy was picked out. Graphs were prepared by open-source Pymol (v.2.6.0a0).

Single-vesicle binding assay

Liposomes containing 73.5% POPC, 20% POPE, 5% PIs, 0.5% Biotin-DPPE, and 1% DiD were first mixed with proper amount in chloroform and dried under nitrogen flow followed by vacuuming for 6 h. Lipid films were dissolved by TBS150 and sonicated for 30 min at a power of 60 W. Sonicated liposomes were then centrifuged at 200× *g* to remove large patches and insoluble fractions. Prepared liposomes were stored at 37 °C in the dark before using.

Homemade chamber for total internal reflection imaging contains a 25 × 75 mm-size, 1 mm-thick glass slide and a 24 × 50 mm-size, 0.13 × 0.16 mm-thick glass coverslip. A number of holes on the slide were drilled by 0.8 mm diamond drill to make 4 channels for each chamber. The drilled slides and coverslips were first washed by sonication in 5% Alconox (Aldrich) for 30 min at 60 W power followed by sonication in actone for 10 min and 1 M NaOH for 1 h at 60 W power. After extensively washed by deionized water, the slides and coverslips were soaked into methanol and burned on an alcohol burner to extinct any potential organic chromophores. Cleaned slides and coverslips were stored at room temperature in 50 mL centrifuge tubes before using.

Before imaging, the slides and coverslips were first siliconized in 100 mL methanol, 5 mL acetic acid, and 1 mL N-[3-(Trimethoxysilyl) propyl]ethylenediamine (Aladdin, #T101385) for 20 min in the dark. After washed by deionized water and dried under nitrogen flow, the slides and coverslips were modified by mPEG-Succinimidyl Valerate, MW 5000 (mPEG-SVA, Laysan Bio, #MPEG-SVA-5000) and Biotin-mPEG-Succinimidyl Valerate, MW 5000 (Biotin-PEG-SVA, Laysan Bio, #Biotin-PEG-SVA-5000) dissolved in 0.1 M $NaHCO_3$ with a ratio of 20:1. In order to exclude non-specific binding of the peptide, another round of modification using mPEG-Succinimidyl Succinate, MW 550 (mPEG-SS, Laysan Bio, #MPEG-SS-550) was applied. All of the functional modification were carried out at 16 °C in the dark for 1 h. The remnant modification buffers were washed extensively by deionized water and the slides and coverslips were dried under nitrogen flow. Modified slides and coverslips were stored in 50 mL centrifuge tubes at room temperature with nitrogen as blanket gas.

The imaging chamber contains a pair of slide and coverslip. Double-sided sticky tape was used as spacers for each channel. The chamber was finally sealed by epoxy. 0.2 mg/mL NeutrAvidin (ThermoFisher, #31000) dissovled in TBS150 buffer was first flowed into the channels in the chamber, after incubation at room temperature for 15 min, 5% (w/v) bovine serum albumin (BSA) in TBS150 was used to wash out remnant neutravidins followed by 20 min incubation at room temperature. Afterwards, 40 μM (total lipids) of liposomes were then flowed into the channel. Washing step using TBS150 was applied after 20 min incubation at room temperature. Finally, EGFP-tagged proteins (200 nM), diluted by imaging buffer that contains TBS150 supplied with 20 units/mL glucose oxidase (from Aspergillus niger, Sigma Aldrich, #G7141), 1000 units/mL catalase (from bovine liver, Sigma Aldrich, #C40), and 1% (w/v) dextrose (Sigma Aldrich, #D9559) to minimize photobleaching, were flowed into specific channels, incubation for 2 h at 25 °C.

Total internal reflection imaging was achieved by using a 100× TIRF objective (NA 1.49, Nikon) on a Nikon Ti inverted microscope equipped with an electronic motored TIRF illuminator, an EMCCD camera (AndoriXon DU987), and two solid-state lasers, Sapphire 488 LP (20 mW, Coherent) and CUBE 640-40 C (40 mW, Coherent). Laser powers were adjusted to 5% and 1% for 488 nm and 640 nm, respectively by acoustic optical modulator (AOM). Images were captured with exposure time of 200 ms. Initially, the liposome density was checked. During the acquisition, each imaging field was acquired alternatively using FITC and Cy5 filter cubes (Chroma).

Codes for data processing were written in MATLAB (v.2017a 9.2.0.538062, MathWorks). Source codes were uploaded to GitHub and could be found at: https://github.com/shenwang3333/slipobinding. The flowchart of data processing is shown in Supplementary information, Fig. S12b. Protein and liposome spots were tracked through finding local maximum pixels. For correlation of liposome sizes and liposome intensities, prepared liposomes were first measured by dynamic light scattering (DLS), designated as DLS model. Summed histograms of single liposome intensities were also counted as intensity distribution. The logarithms of two statistical results were fitted to Gaussian amplitude function:

$$G(t) = g_{\text{offset}} + A * \exp\left(-\frac{\left(\frac{t-t_c}{\sigma}\right)^2}{2}\right)$$

where t_c is the center/mean value of Gaussian amplitude distribution. For the two distributions that possess comparable σ^2, the convert factor could be applied to convert intensities to diameters measured by DLS:

$$f_c = x_c^{DLS}/x_c^{Intensity}$$

Since the protein channels have poor signal-to-noise ratio (SNR), we applied band-pass filter for each of the protein channel captures. During each processing rounds, a protein channel capture was sent to spots detection, then the coordinates of spot centers, spot scales, and spot densities (total intensity divided by pixel areas) were listed and stored. Using the xy-coordinates and spot scales list of the protein spots as a guide, we could extract the liposome intensities in exactly the same place from the corresponding liposome capture. By virtue of the correlation of liposome sizes and liposome intensities, we could calculate the binding densities (D) of proteins to each single liposome:

$$D = \frac{\sum I_{prot}}{4\pi\left(\sum I_{lipo} f_c\right)^2}$$

where $\sum I_{prot}$ is the intensity sum of a detected protein spot and $\sum I_{lipo}$ is the intensity sum of a detected liposome spot at the same place.

Sequence alignment

Sequence alignment was performed by Clustal Omega (v1.2.4) and visualized by ESPript 3.0 (https://espript.ibcp.fr/ESPript/ESPript/). Secondary structure elements were from the predicted structure of human SNAP47-PH. Protein sequences of SNAP47 in different species were fetched from Uniprot (https://www.uniprot.org/).

Statistical analysis

Statistical analysis was carried out on the data from independent experiments using Prism software (GraphPad). The error bars in the figures represent SD or SEM. Unpaired *t*-tests, one-way ANOVA, and two-way ANOVA were performed for statistical analysis. At least 3 repeats were performed for each experiment. The statistical information of each experiment, including the statistical methods, significance and numbers were shown in the figures and corresponding legends.

DATA AVAILABILITY

All data are available in the main text or the supplementary materials.

REFERENCES

1. Morishita, H. & Mizushima, N. Diverse cellular roles of autophagy. *Annu. Rev. Cell Dev. Biol.* **35**, 453–475 (2019).
2. Huang, Y. J. & Klionsky, D. J. Yeast mitophagy: Unanswered questions. *Biochim. Biophys. Acta Gen. Subj.* **1865**, 129932 (2021).
3. Moehlman, A. T. & Youle, R. J. Mitochondrial quality control and restraining innate immunity. *Annu. Rev. Cell Dev. Biol.* **36**, 265–289 (2020).
4. Sarraf, S. A. & Youle, R. J. Parkin mediates mitophagy during beige-to-white fat conversion. *Sci. Signal.* **11**, eaat1082 (2018).
5. Pickles, S., Vigie, P. & Youle, R. J. Mitophagy and quality control mechanisms in mitochondrial maintenance. *Curr. Biol.* **28**, R170–R185 (2018).
6. Jahn, R. & Scheller, R. H. SNAREs-engines for membrane fusion. *Nat. Rev. Mol. Cell Biol.* **7**, 631–643 (2006).
7. Itakura, E., Kishi-Itakura, C. & Mizushima, N. The hairpin-type tail-anchored SNARE syntaxin 17 targets to autophagosomes for fusion with endosomes/lysosomes. *Cell* **151**, 1256–1269 (2012).
8. Takats, S. et al. Autophagosomal Syntaxin17-dependent lysosomal degradation maintains neuronal function in Drosophila. *J. Cell Biol.* **201**, 531–539 (2013).
9. Diao, J. et al. ATG14 promotes membrane tethering and fusion of autophagosomes to endolysosomes. *Nature* **520**, 563–566 (2015).
10. Matsui, T. et al. Autophagosomal YKT6 is required for fusion with lysosomes independently of syntaxin 17. *J. Cell Biol.* **217**, 2633–2645 (2018).
11. Takáts, S. et al. Non-canonical role of the SNARE protein Ykt6 in autophagosome–lysosome fusion. *PLoS Genet.* **14**, e1007359 (2018).
12. Bas, L. et al. Reconstitution reveals Ykt6 as the autophagosomal SNARE in autophagosome-vacuole fusion. *J. Cell Biol.* **217**, 3656–3669 (2018).
13. Gao, J., Reggiori, F. & Ungermann, C. A novel in vitro assay reveals SNARE topology and the role of Ykt6 in autophagosome fusion with vacuoles. *J. Cell Biol.* **217**, 3670–3682 (2018).
14. Katayama, H., Kogure, T., Mizushima, N., Yoshimori, T. & Miyawaki, A. A sensitive and quantitative technique for detecting autophagic events based on lysosomal delivery. *Chem. Biol.* **18**, 1042–1052 (2011).
15. Pankiv, S. et al. p62/SQSTM1 binds directly to Atg8/LC3 to facilitate degradation of ubiquitinated protein aggregates by autophagy. *J. Biol. Chem.* **282**, 24131–24145 (2007).
16. Szeto, J. et al. ALIS are stress-induced protein storage compartments for substrates of the proteasome and autophagy. *Autophagy* **2**, 189–199 (2006).
17. Fan, W. et al. Keap1 facilitates p62-mediated ubiquitin aggregate clearance via autophagy. *Autophagy* **6**, 614–621 (2010).
18. Ma, X. et al. CCT2 is an aggrephagy receptor for clearance of solid protein aggregates. *Cell* **185**, 1325–1345.e22 (2022).
19. Lemmon, M. A. Membrane recognition by phospholipid-binding domains. *Nat. Rev. Mol. Cell Biol.* **9**, 99–111 (2008).
20. Nguyen, T. N. et al. Atg8 family LC3/GABARAP proteins are crucial for autophagosome–lysosome fusion but not autophagosome formation during PINK1/Parkin mitophagy and starvation. *J. Cell Biol.* **215**, 857–874 (2016).
21. Guo, B. et al. O-GlcNAc-modification of SNAP-29 regulates autophagosome maturation. *Nat. Cell Biol.* **16**, 1215–1226 (2014).
22. Yu, L., Chen, Y. & Tooze, S. A. Autophagy pathway: Cellular and molecular mechanisms. *Autophagy* **14**, 207–215 (2018).
23. Nakamura, S., Hasegawa, J. & Yoshimori, T. Regulation of lysosomal phosphoinositide balance by INPP5E is essential for autophagosome–lysosome fusion. *Autophagy* **12**, 2500–2501 (2016).
24. Chen, D. et al. A mammalian autophagosome maturation mechanism mediated by TECPR1 and the Atg12-Atg5 conjugate. *Mol. Cell* **45**, 629–641 (2012).
25. Wang, H. et al. GABARAPs regulate PI4P-dependent autophagosome:lysosome fusion. *Proc. Natl. Acad. Sci. USA* **112**, 7015–7020 (2015).
26. Sun, H. Q. et al. PI4P-dependent targeting of ATG14 to mature autophagosomes. *Biochemistry* **61**, 722–729 (2022).
27. Wu, Y. et al. PI3P phosphatase activity is required for autophagosome maturation and autolysosome formation. *EMBO Rep.* **15**, 973–981 (2014).
28. Moreau, K., Ravikumar, B., Puri, C. & Rubinsztein, D. C. Arf6 promotes autophagosome formation via effects on phosphatidylinositol 4,5-bisphosphate and phospholipase D. *J. Cell Biol.* **196**, 483–496 (2012).
29. Tan, X., Thapa, N., Liao, Y., Choi, S. & Anderson, R. A. PtdIns(4,5)P2 signaling regulates ATG14 and autophagy. *Proc. Natl. Acad. Sci. USA* **113**, 10896–10901 (2016).
30. Fan, W., Nassiri, A. & Zhong, Q. Autophagosome targeting and membrane curvature sensing by Barkor/Atg14(L). *Proc. Natl. Acad. Sci. USA* **108**, 7769–7774 (2011).
31. Zhang, H. et al. PtdIns4P restriction by hydrolase SAC1 decides specific fusion of autophagosomes with lysosomes. *Autophagy* **17**, 1907–1917 (2021).
32. Baba, T., Toth, D. J., Sengupta, N., Kim, Y. J. & Balla, T. Phosphatidylinositol 4,5-bisphosphate controls Rab7 and PLEKHM1 membrane cycling during autophagosome–lysosome fusion. *EMBO J.* **38**, e100312 (2019).
33. De Leo, M. G. et al. Autophagosome–lysosome fusion triggers a lysosomal response mediated by TLR9 and controlled by OCRL. *Nat. Cell Biol.* **18**, 839–850 (2016).
34. Zhao, Y. G., Codogno, P. & Zhang, H. Machinery, regulation and pathophysiological implications of autophagosome maturation. *Nat. Rev. Mol. Cell Biol.* **22**, 733–750 (2021).
35. Nakamura, S. & Yoshimori, T. New insights into autophagosome–lysosome fusion. *J. Cell Sci.* **130**, 1209–1216 (2017).
36. Kumar, S. et al. Mammalian Atg8 proteins and the autophagy factor IRGM control mTOR and TFEB at a regulatory node critical for responses to pathogens. *Nat. Cell Biol.* **22**, 973–985 (2020).
37. Gu, Y. et al. Mammalian Atg8 proteins regulate lysosome and autolysosome biogenesis through SNAREs. *EMBO J.* **38**, e101994 (2019).
38. Kumar, S. et al. Mechanism of Stx17 recruitment to autophagosomes via IRGM and mammalian Atg8 proteins. *J. Cell Biol.* **217**, 997–1013 (2018).
39. Sagiv, Y., Legesse-Miller, A., Porat, A. & Elazar, Z. GATE-16, a membrane transport modulator, interacts with NSF and the Golgi v-SNARE GOS-28. *EMBO J.* **19**, 1494–1504 (2000).
40. Wang, Y. et al. ULK phosphorylation of STX17 controls autophagosome maturation via FLNA. *J. Cell Biol.* **222**, e202211025 (2023).
41. Zhao, Y. G. & Zhang, H. Autophagosome maturation: An epic journey from the ER to lysosomes. *J. Cell Biol.* **218**, 757–770 (2019).
42. Wang, Z. et al. The Vici Syndrome Protein EPG5 Is a Rab7 effector that determines the fusion specificity of autophagosomes with late endosomes/lysosomes. *Mol. Cell* **63**, 781–795 (2016).
43. McEwan, D. G. et al. PLEKHM1 regulates autophagosome–lysosome fusion through HOPS complex and LC3/GABARAP proteins. *Mol. Cell* **57**, 39–54 (2015).
44. Wang, Y., Que, H. & Rong, Y. Autophagosomal components recycling on autolysosomes. *Trends Cell Biol.* **32**, 897–899 (2022).

45. Koyama-Honda, I., Tsuboyama, K. & Mizushima, N. ATG conjugation-dependent degradation of the inner autophagosomal membrane is a key step for autophagosome maturation. *Autophagy* **13**, 1252–1253 (2017).
46. Tan, H. W. S. et al. A degradative to secretory autophagy switch mediates mitochondria clearance in the absence of the mATG8-conjugation machinery. *Nat. Commun.* **13**, 3720 (2022).
47. Jiao, H. et al. Mitocytosis, a migrasome-mediated mitochondrial quality-control process. *Cell* **184**, 2896–2910.e13 (2021).
48. Bao, F. et al. Mitolysosome exocytosis, a mitophagy-independent mitochondrial quality control in flunarizine-induced parkinsonism-like symptoms. *Sci. Adv.* **8**, eabk2376 (2022).
49. Liang, W. et al. Mitochondria are secreted in extracellular vesicles when lysosomal function is impaired. *Nat. Commun.* **14**, 5031 (2023).
50. Kuster, A. et al. The Q-soluble N-Ethylmaleimide-sensitive Factor Attachment Protein Receptor (Q-SNARE) SNAP-47 regulates trafficking of selected Vesicle-associated Membrane Proteins (VAMPs). *J. Biol. Chem.* **290**, 28056–28069 (2015).
51. Matsui, T., Sakamaki, Y., Hiragi, S. & Fukuda, M. VAMP5 and distinct sets of cognate Q-SNAREs mediate exosome release. *Cell Struct. Funct.* **48**, 187–198 (2023).
52. Dietrich, L. E., Boeddinghaus, C., LaGrassa, T. J. & Ungermann, C. Control of eukaryotic membrane fusion by N-terminal domains of SNARE proteins. *Biochim. Biophys. Acta* **1641**, 111–119 (2003).
53. Martinez-Arca, S., Alberts, P., Zahraoui, A., Louvard, D. & Galli, T. Role of tetanus neurotoxin insensitive vesicle-associated membrane protein (TI-VAMP) in vesicular transport mediating neurite outgrowth. *J. Cell Biol.* **149**, 889–900 (2000).
54. Tochio, H., Tsui, M. M., Banfield, D. K. & Zhang, M. An autoinhibitory mechanism for nonsyntaxin SNARE proteins revealed by the structure of Ykt6p. *Science* **293**, 698–702 (2001).
55. Vivona, S. et al. The longin SNARE VAMP7/TI-VAMP adopts a closed conformation. *J. Biol. Chem.* **285**, 17965–17973 (2010).
56. Uematsu, M., Nishimura, T., Sakamaki, Y., Yamamoto, H. & Mizushima, N. Accumulation of undegraded autophagosomes by expression of dominant-negative STX17 (syntaxin 17) mutants. *Autophagy* **13**, 1452–1464 (2017).

ACKNOWLEDGEMENTS

We are deeply grateful to Dr. Li Yu (Tsinghua University) and Yuhai Jia (Nanjing Normal University) for helpful suggestions on this study. We thank Dr. Michael Lazarou (Monash University) for sharing ATG8 KO cell lines. We thank Dr. Liang Ge (Tsinghua University) for sharing the HTT(Q103) plasmid. The work was supported by grants from NSFC (92254302, 91854116, 32170685 and 31771529 to Y.R.). The work was partially supported by the Fundamental Research Funds for the Central Universities (5003510089 and 2023BR028 to Y.R.).

AUTHOR CONTRIBUTIONS

F.J. and Y.R. conceived and designed the biological and biochemical experiments. F.J., R.T., Y.W., and C.L. carried out the biological and biochemical experiments. S.W. C.M. and Y.R. designed and S.W. carried out the in vitro liposome fusion and single vesicle binding experiments. F.J., S.W., C.M., C.F., Y.L., S.X.W. and Y.R. analyzed the data and wrote the manuscript with the help of all authors.

COMPETING INTERESTS

The authors declare no competing interests.

ADDITIONAL INFORMATION

Supplementary information The online version contains supplementary material available at https://doi.org/10.1038/s41422-023-00916-x.

Correspondence and requests for materials should be addressed to Cong Ma or Yueguang Rong.

Reprints and permission information is available at http://www.nature.com/reprints

Springer Nature or its licensor (e.g. a society or other partner) holds exclusive rights to this article under a publishing agreement with the author(s) or other rightsholder(s); author self-archiving of the accepted manuscript version of this article is solely governed by the terms of such publishing agreement and applicable law.